HHS Public Access

Author manuscript

Acta Biomater. Author manuscript; available in PMC 2020 May 15.

Published in final edited form as:

Acta Biomater. 2019 September 15; 96: 330–344. doi:10.1016/j.actbio.2019.07.002.

Effects of gamma radiation sterilization on the structural and biological properties of decellularized corneal xenografts

Mohammad Mirazul Islam[a], **Roholah Sharifi**[a], **Shamina Mamodaly**[a], **Rakibul Islam**[b], **Daniel Nahra**[a], **Dina B. Abusamra**[a], **Pui Chuen Hui**[a], **Yashar Adibnia**[a,c], **Mehdi Goulamaly**[d], **Eleftherios I. Paschalis**[a], **Andrea Cruzat**[a,e], **Jing Kong**[d], **Per H. Nilsson**[b,f], **Pablo Argüeso**[a], **Tom Eirik Mollnes**[b,g,h], **James Chodosh**[a], **Claes H. Dohlman**[a], **Miguel Gonzalez-Andrades**[a,i,*]

[a]Massachusetts Eye and Ear and Schepens Eye Research Institute, Department of Ophthalmology, Harvard Medical School, Boston, MA, USA

[b]Department of Immunology, Oslo University Hospital, Rikshospitalet, University of Oslo, Oslo, Norway

[c]Yeditepe University School of Medicine, Istanbul, Turkey

[d]Department of Electrical Engineering and Computer Science, Massachusetts Institute of Technology, Cambridge, MA, USA

[e]Department of Ophthalmology, Pontificia Universidad Católica de Chile, Santiago, Chile

[f]Linnaeus Center for Biomaterials Chemistry, Linnaeus University, Kalmar, Sweden

[g]Research Laboratory, Nordland Hospital, Bodø, and Faculty of Health Sciences, K.G. Jebsen TREC, University of Tromsø, Norway

[h]Centre of Molecular Inflammation Research, Norwegian University of Science and Technology, Trondheim, Norway

[i]Maimonides Biomedical Research Institute of Cordoba (IMIBIC), Department of Ophthalmology, Reina Sofia University Hospital and University of Cordoba, Cordoba, Spain

Abstract

To address the shortcomings associated with corneal transplants, substantial efforts have been focused on developing new modalities such as xenotransplantion. Xenogeneic corneas are anatomically and biomechanically similar to the human cornea, yet their applications require prior decellularization to remove the antigenic components to avoid rejection. In the context of bringing decellularized corneas into clinical use, sterilization is a crucial step that determines the success of

*Corresponding author at: Massachusetts Eye and Ear - Schepens Eye Research Institute, 20 Staniford St, Boston, MA 02114, USA. miguel_gonzalez@meei.harvard.edu (M. Gonzalez-Andrades).

Disclosures

Mohammad Mirazul Islam, Roholah Sharifi, Dina B. Abusamra, Pui Chuen Hui, Eleftherios I. Paschalis, Andrea Cruzat, Pablo Argüeso, James Chodosh, Claes H. Dohlman and Miguel Gonzalez-Andrades are, or were in the past, full-time employees of Massachusetts Eye and Ear, Boston – the manufacturer of the Boston Keratoprosthesis.

The datasets generated during and/or analyzed during the current study are available from the corresponding author on reasonable request.

Appendix A. Supplementary material

Supplementary data to this article can be found online at https://doi.org/10.1016/j.actbio.2019.07.002.

the transplantation. Well-standardized sterilization methods, such as gamma irradiation (GI), have been applied to decellularized porcine corneas (DPC) to avoid graft-associated infections in human recipients. However, little is known about the effect of GI on decellularized corneal xenografts. Here, we evaluated the radiation effect on the ultrastructure, optical, mechanical and biological properties of DPC. Transmission electron microscopy revealed that gamma irradiated decellularized porcine cornea (G-DPC) preserved its structural integrity. Moreover, the radiation did not reduce the optical properties of the tissue. Neither DPC nor G-DPC led to further activation of complement system compared to native porcine cornea when exposed to plasma. Although, DPC were mechanically comparable to the native tissue, GI increased the mechanical strength, tissue hydrophobicity and resistance to enzymatic degradation. Despite these changes, human corneal epithelial, stromal, endothelial and hybrid neuroblastoma cells grew and differentiated on DPC and G-DPC. Thus, GI may achieve effective tissue sterilization without affecting critical properties that are essential for corneal transplant survival.

Keywords

Gamma irradiation sterilization; Decellularization; Corneal transplant; Recellularization; Acellular porcine cornea

1. Introduction

Corneal diseases are one of the leading causes of blindness in the world [1]. In severe cases, corneal transplantation is the most used and reliable treatment [2]. However, most of the world population, including 90% of the visually impaired people, live in low-income countries, where a severe shortage of donor corneas and a lack of readiness for corneal transplantation exists [1,3]. In total, 12.7 million people worldwide are waiting for a corneal transplant [4]. Although corneal transplantation is considered the most successful organ transplant procedure, it is associated with two major complications; immune rejection and donor-derived infections [5,6]. Microbial screening and administrative cost for shipping donor corneas make corneal allograft surgery an unaffordable treatment option for most patients world-wide [7]. Thus, to compensate for the scarcity of human donor corneas and to overcome the cost and major complications of corneal transplantation, appropriate alternatives are needed. In this context, xenografts emerge as a real possibility to replace human donor corneas. Corneas from pigs [8], rabbits [9], gibbons [10], cows [11], chickens [12], monkeys [12] and fishes [13] were transplanted into humans during the early stages of xenotransplantation with very limited success. In all the cases, the implant failed mainly due to host immune reaction against graft [14]. Thus, complete or partial removal of donor cellular components that initiate immune reactions and activate the complement system is important for the survival of xenografts transplanted in humans [15]. Furthermore, cross-species infectious diseases are another major complication of xenograft transplantation that need to be addressed [16].

Not only for the cornea but for many other tissues and organs, decellularization has become a promising approach to overcome the major complications of xenograft transplantation. Moreover, the decellularized organs can be used as scaffolds for tissue regeneration that

maintain physiological properties required to replace the target organ [17]. Regarding the cornea, the pig (*Sus scrofa domesticus*) has been the most widely used species because of the anatomical and physiological similarities to humans [18,19], including composition and structure of corneal stromal proteins [20]. A number of methods have been developed to decellularize porcine corneas (DPC) [21,22]. Most of these use detergents, such as sodium dodecyl sulfate (SDS), or induce osmotic changes with NaCl. Although detergents are cytotoxic and need to be washed out fully from the xenograft, they are widely used to decellularize because their use is simple and inexpensive. Moreover, detergents can easily be combined with other decellularization methods, such as NaCl, to improve the efficiency of the protocol [23]. In our previous work, we demonstrated the efficacy of NaCl and SDS to generate DPC after treatment with dispase II [24] and further determined the decellularizing effect of benzalkonium chloride, Igepal, SDS or Triton X-100 at different concentrations and different time intervals [22]. Other decellularization techniques have been described, such as high hydrostatic pressure and supercritical carbon dioxide, but they all require expensive and specialized equipment [25,26].

In the context of bringing decellularized corneas into clinical use, sterilization is a critical step. Well-standardized sterilization methods, such as gamma irradiation (GI), have been applied to decellularized xenografts to avoid graft-associated infections in human recipients [27]. Tissue banks commonly use GI for sterilization of tissues and biological substances against bacterial, viral, fungal and prional contamination [28,29]. GI has also been applied successfully to human corneas. Most of patients that received a gamma irradiated human cornea showed favorable outcomes without graft rejection, loss of transparency or neovascularization [30]. Moreover, GI might reduce allogenicity [31], with the added advantage of a shelf life of the sterile irradiated human cornea for more than one year at room temperature [32]. However, little is known about the effect of GI on DPC despite of the recent use of these xenografts in high-risk patients with infectious keratitis [23,27].

Thus, there is a critical need for evaluating the effect of GI on the ultrastructure, optical, mechanical and biological properties of DPC in order to facilitate its translation into the clinical practice. In the present work, we optimized the decellularization of porcine corneas using SDS in distilled water (dH_2O) and sterilization with 25 kGy of GI. We evaluated biocompatibility and *in vitro* complement activation of DPC before and after GI. Furthermore, the optical and mechanical properties were investigated as well as the feasibility of implanting this tissue in *ex vivo* models of keratoplasty and keratoprosthesis.

2. Materials and methods

2.1. Preparation of decellularized porcine corneas (DPC)

Fresh porcine eyes were obtained from adult pigs immediately after their death at a local slaughterhouse. After receiving the eyes, corneas were inspected with a portable slit lamp (S150, Medi-Works Precision Instruments; Shanghai, China) to discard those showing any corneal damage. Selected corneas were removed from pig eyes with a 16-mm-diameter trephine and washed with phosphate buffer saline (PBS). In every experiment, native porcine corneas (NPC) without further processing for decellularization were used as control. These control corneas were immediately fixed and went for further processing. For

decellularization, corneas were placed in a 6-well plate, facing epithelial side down (1 cornea per well). 0.1% SDS (Applied Biosystems, CA, USA) buffer in dH_2O was added to the wells. After 72 h, SDS was replaced by PBS and maintained for 48 h. All the solutions were 5 ml in volume and changed every 24 h. NPC in dH_2O for 72 h served as a secondary control of this study. The complete decellularization process was carried out under continuous shaking (70 rpm) at room temperature. Finally, DPC were immersed into 100% glycerol (5 ml) for dehydration and kept at room temperature without shaking until further use.

2.2. Evaluation of decellularization efficiency

For histological evaluation, NPC and DPC were fixed in 4% paraformaldehyde, dehydrated in increasing concentrations of ethanol (70%, 96%, 100%) for 30 min at each concentration. The tissues were immersed twice in xylene for 30 min and then kept in liquid paraffin for 30 min. Paraffin-embedded sections were cut to 6 μm thickness with a microtome and stained for histology with hematoxylin for 2 min and eosin for 1 min (H&E, Hematoxylin Stain, Fisher Chemical, NJ, USA and Eosin Y, Fisher Chemical). Staining with 1% Alcian blue (AB, Electron Microscopy Science, PA, USA) for 30 min was done to visualize the glycosaminoglycans (GAG) [33]. Staining with Periodic acid–Schiff (PAS, Fisher Chemical) for 15 min together with counterstain of hematoxylin for 1 min was performed to detect the presence of polysaccharides, principally glycogen [34].

To determine the decellularization efficiency, the number and area of remaining nuclei and nuclear debris in NPC and DPC (3 corneas per group) were quantified by using 4,6-diamidino-2-phenylindole (DAPI) staining (VectaShield mounting medium containing DAPI - Vector Laboratories, Inc., CA, USA) on deparaffinized tissue sections and the percentage of cell removal was determined. 3 sections per cornea were analyzed. To capture representative pictures of the entire corneal stroma of every sample, we devised a specific protocol for photography that ran from anterior to posterior of the cornea at 10X magnification, obtaining at least 6 pictures per section with a fluorescence microscope (Zeiss Axio Observer Z1, Carl Zeiss Microimaging GmbH, Jena, Germany). The microscope settings were kept constant across samples. The number of remaining nuclei and nuclear debris was determined per image using the analyze particle function of ImageJ (Maryland, USA), after applying a specific threshold (20, 255) and establishing specific size particle ranges (1.00–6.99 $pixels^2$ for nuclear debris and 7.00–1000.00 $pixels^2$ for nuclei).

The presence of alpha Gal (α-gal) epitopes and N-glycolylneuraminic acid (NeuGc), including collagen type I, in NPC and DPC was evaluated by Western blot (WB). Corneas from each group were homogenized in Triton X-100 lysis buffer (0.5% Triton X-100, 50 mM-Tris base -pH 8.0-, 150 mM NaCl, 1 mM PMSF and protease inhibitor cocktail tablet) (Roche Diagnostics GmbH, Mannheim, Germany) using a three round of sonication for 10 s each and followed by five rounds of freeze and thaw. Loaded lysates were normalized to equal protein concentration using Pierce™ BCA Protein Assay Kit (Thermo scientific, IL, USA). WB membranes were immune-stained with α-gal mouse monoclonal antibody (clone M86, ALX-801–090-1, Enzo Life Science, dilution 1:5), anti-Neu5Gc chicken polyclonal antibody (clone Poly21469, 146903, BioLegend Inc., dilution 1:1000) and anti-collagen I

monoclonal mouse antibody (clone COL-1, ab90395, Abcam, dilution 1:500) followed by the appropriate horseradish peroxidase secondary antibody (Abcam, Cambridge, UK). Band intensities were quantified by densitometry (ImageJ software; National Institutes of Health, Bethesda, MD). Normalization was done using corresponding collagen expression as internal control.

2.3. Gamma sterilization of decellularized porcine corneas (DPC)

GI was performed to sterilize DPC, using a cobalt-60 source (MDS Nordion Gammacell 220E irradiator, at the Massachusetts Institute of Technology Department of Biological Engineering; Cambridge, MA). The samples were individually packaged in sealed glass vials filled with glycerol. The vials were placed centrally in the irradiator chamber for GI at room temperature. The dose was calculated according to cobalt-60 source decay calculation. International Atomic Energy Agency (IAEA) recommends 25 kGy as the standard dose when the natural contamination level and microorganism types cannot be calculated, because this dose provides a maximum sterility assurance level of 10^{-6} [35]. In accordance, we used 25 kGy for the sterilization of DPC.

2.4. Transmission electron microscopy (TEM)

Transmission electron microscopy (TEM) was performed on native human corneas (NHC), NPC, DPC and gamma irradiated DPC (G-DPC) samples. All corneal samples were fixed with half strength Karnovsky's fixative (pH 7.4) (Electron Microscopy Sciences, Hatfield, Pennsylvania) at room temperature for 30 min, and then placed in fresh Karnovsky's fixative for 4 h. The samples were washed with 0.1 M Cacodylate Buffer (Electron Microscopy Sciences, Hatfield, Pennsylvania) for 5 min at room temperature, and again three times. After washing with PBS, specimens were post-fixed using 2% osmium tetroxide (Electron Microscopy Sciences) for 1.5 h at room temperature. Subsequently, the specimens were *en bloc* stained with 2% aqueous uranyl acetate for 30 min, then dehydrated with ethanol, and embedded in epoxy resin (Tousimis, Rockville, Maryland, USA). Ultrathin sections (80 nm) were cut from each sample block using a Leica EM UC7 ultramicrotome (Leica Microsystems, Buffalo Grove, IL, USA) and a diamond knife, and mounted on grids. Thin sections on grids were stained with aqueous 2.5% aqueous gadolinium (III) acetate hydrate and Sato's lead citrate stains using a modified Hiraoka grid staining system [36]. Sections were observed by TEM with accelerating voltage at 80 kV (FEI Tecnai G2 Spirit transmission electron microscope, FEI, Hillsboro, Oregon, USA).

2.5. Evaluation of optical properties

The optical properties of the native and treated corneas were assessed by a UV–Vis spectrometer (Molecular Devices SpectraMax 384 Plus Microplate Reader, CA, USA). Briefly, 6-mm-diameter central corneal pieces were trephined from NPC, DPC and G-DPC. Subsequently, the cornea pieces were placed in a 96-well quartz microplate filled with glycerol, and the spectral transmittance of each sample was measured using the UV–Vis spectrometer. The transmittance data were recorded at 1 nm wavelength increments, from 250 to 850 nm. Experiments were performed five times and transmittance of the samples was corrected with glycerol as a blank media in a quartz microplate and the mean percentage of transmittance for each group calculated and plotted as a function of wavelength.

2.6. Polarization-sensitive optical coherence tomography

A custom-built bench-top polarization-sensitive optical coherence tomography (PS-OCT) system was used to examine the depth-resolved optical polarization properties of the corneas, following the procedure previously described [37,38], in order to complement the TEM approach in Section 2.4 and evaluate the collagen fibril organization in the different corneal samples mesoscopically over a large field of view. The cornea shows optical birefringence because of its characteristic orientated lamellar structure [39]. Corneas (Intact NPC, NPC, DPC and G-DPC) were rehydrated in PBS for 10 min before imaging. The optical birefringence, which is the difference in the refractive indices of light polarized in two different directions, can be measured by irradiating the samples using incident light of linear and circular polarizations and detecting the backscattered light using a polarization-diverse detection module [40]. The intensity image was obtained via standard Fourier-transform demodulation procedures. The depth-resolved birefringence map was further reconstructed by evaluating the Stokes' vectors and employing a spectral-binning technique [40]. To enhance the contrast of the map, we only report the birefringence values in areas with a sufficiently high degree of polarization. Additionally, central corneal thickness of NPC, DPC and G-DPC was measured using PS-OCT images (n = 6), considering the tissue refractive index (1.38).

2.7. Evaluation of mechanical properties

The ultimate tensile strength, elongation at break and elastic modulus of the corneal tissue were measured using a Mark-10 ESM 303 (Mark-10 Corporation, NY, USA) equipped with MESUR Gauge Plus software. The instrument was equipped with a load cell of 50 N, crosshead speed was 0.5 mm/min and the initial grip separation was 6 mm. Corneal tissues (NHC, NPC, DPC and G-DPC) were dissected into dumbbell-shaped samples of the total length of 12 mm, a gage section of 4×4 mm and griping width of 6 mm. The serrated steel jaws of self-tightening grips avoided any slippage of the sample in the jaws. Samples were stress-freed prior to testing and each reported value represents the average of at least four measurements using four independent corneas. The Compression Modulus was also assessed by subjecting 6-mm-diameter discs from the same three groups to compressive-strength measurements using a Mark-10 ESM 303 (Mark-10 Corporation, NY, USA) at a constant speed of 0.5 mm/min. For testing, the tissue discs were preserved in PBS at room temperature immediately prior to the measurement.

2.8. Water content measurement

The water content was measured on DPC, G-DPC and NPC. All the corneas were soaked in glycerol for two days to keep the conditions constant between the control and the DPC, and then rehydrated with PBS for 2 h. The wet weights of the corneas were measured after blotting with a filter paper to remove any surface water. Dry weights of all the corneas were taken after 24 h of lyophilization. The hydrated mass ($m_{hydrated}$) and the dry mass (m_{dry}) were used to determine the water content by using the following equation.

$$\text{Water content} = \left\{\left(m_{hydrated} - m_{dry}\right)/m_{hydrated}\right\} \times 100$$

2.9. Contact angle measurement

The surface hydrophilicity of different corneal samples - NPC, NPC where the epithelium was removed by scraping with a surgical blade (D-NPC), DPC and G-DPC - were studied by contact angle measurement. D-NPC was evaluated to understand the direct effect of the absence of corneal epithelium on contact angle. It has been suggested that angles ranging from 40 to 60 degrees might be correlated with the promotion of cell adhesion [41]. For that purpose, the corneas were punched with a 5 mm trephine and washed in PBS for 15 min by vigorous shaking. Afterwards, the surface of the corneas was placed in between Whatman Quantitative Filter Papers, Ashless Grades (ash 0.007%), Grade 42 and pressed under a glass slide to remove the excess PBS and flatten the cornea. The flattening process consisted of putting a 2.5 kg weight on top of the sample for 30 min. The samples were then put onto the contact angle measuring equipment (ramé-hart Model 590 Automated Goniometer/ Tensiometer (p/n 590-U1) Ledgewood, NJ, USA). A 2 μl drop of dH_2O was deposited onto the corneas by a micro-syringe and the contact angle was measured. Each measurement was performed in less than 1 s in order to avoid any significant impact of evaporation on the measurements. Ten pictures were taken within 1 s and the average contact angle of the 10 images was computed by the DROPimage Advanced software (Ramé-hart instrument co. Succasunna, NJ, USA).

2.10. Glucose diffusivity measurements

The Static Franz cell system composed of 1 ml upper cell cap and a 5 ml lower receptor chamber with a diameter of 9 mm (PermeGear 6G-01–00-09–05, PA, USA) made from borosilicate glass was used to assess the permeability of the corneal samples. 15-mm-diameter discs from fresh and treated porcine corneas (NPC, DPC and G-DPC) were prepared and inserted between the two compartments, creating a barrier between the two chambers. The upper compartment was filled with 1 ml PBS and the bottom chamber was filled with a glucose solution (5 ml PBS with a glucose content of 2000 mg/dl). Both chambers were equipped with a small stirrer bar, and the solutions were mixed with a magnetic stirrer throughout the experiment, while the entire unit was placed inside of an incubator at 37 C to allow the diffusion. The glucose concentration in the upper chamber was assessed using a Counter Next EZ blood glucometer (Bayer, Parsippany, NJ, USA) using test strips at different time point. The diffusion coefficients were calculated for each tissue samples using the method previously described by Myung et al. [42].

2.11. In vitro biodegradation study

The resistance of DPC and G-DPC to enzymatic degradation was evaluated using collagenase from *Clostridium histolyticum* (Sigma-Aldrich, St. Louis, USA), following a previously described protocol [43]. In brief, differently treated corneas were placed separately in vials containing 5 U/ml collagenase in 0.1 M Tris-HCl (pH 7.4) buffer supplemented with 5 mM $CaCl_2$ and incubated at 37 C. Corneas were kept in the Tris-HCl buffer at 37 C for 1 h before adding collagenase solution to achieve the equilibrium of the hydration. The collagenase solution was changed every 8 h and the percent residual mass of the sample was measured at different time points by using the following equation:

$$\text{Residual mass } \% = W_t/W_o\%$$

Here W_t is the weight of the sample at a certain time point and W_o is the initial weight of the sample.

2.12. In-vitro human plasma incubation for detection of complement activation

To prepare plasma, whole blood was collected from six healthy donors in 4.5 ml sterile tubes containing the anticoagulant lepirudin (Refludan®; Pharmion ApS, Copenhagen, Denmark) at a final concentration of 50 μg/ml [44]. The collected blood was centrifuged immediately at 3000 × g for 15 min at 4 °C and 100 μl of fresh plasma from the respective donor was incubated with 6-mm-diameter NPC, DPC and G-DPC. Incubations were carried out in 1.8 ml round-bottom sterile polypropylene NUNC cryotubes (Nunc, Roskilde, Denmark) for 30 min at 37 °C. A parallel incubation with 100 μl plasma was kept for thirty minutes (T30) under the same conditions to evaluate background activation. After incubation, the further complement activation was stopped by adding EDTA (20 mM final concentration) and stored at −80 °C until analysis for complement activation products. The complement activation products C4 (C4bc), C3 (C3bc) and the terminal C5–9 pathway (sC5b-9) were analyzed according as previously described [45], and as validated in several *in vivo* studies [46]. Briefly, the assays were based on capture monoclonal antibodies detecting neo-epitopes exposed in the activation products after activation, hence, specifically measuring only the activation products and not the native components.

2.13. In vitro recellularization

2.13.1. Human corneal epithelial cells (HCEC)—The recellularization potentials of DPC and G-DPC were tested using SV40-immortalized HCEC, kindly provided by Professor May Griffith, and as previously published [47]. HCEC grew showing a cobblestone-like appearance similar to normal corneal epithelial cells in culture. TEM showed that this cell line expresses characteristics of epithelial cells, including desmosome formation and development of microvilli. HCEC expressed cornea epithelial cell specific 64-kD cytokeratin. Moreover, this cell line can stratify when cultured at the air-liquid interface on collagen substrates [48].

6-mm-diameter DPC and G-DPC were cut and immersed in keratinocyte serum free-medium (KSFM) at 37 °C for seven days. 50,000 HCEC were seeded on top of each DPC and cultured with KSFM supplemented with 50 μg/ml bovine pituitary extract and 5 ng/ml epidermal growth factor (EGF) (Gibco, California, USA) in a 37 °C and 5% CO_2 incubator. At confluence, live/dead staining was performed with a staining kit (Life Technologies Corporation, Oregon, USA), where cells were double-stained by calceinacetoxymethyl (Calcein AM) and ethidium homodimer-1 (EthD-1). On live culture, to promote stratification after confluence, the media was changed to DMEM/Ham's F-12 media (Corning, VA, USA) supplemented with 10% newborn calf serum and 10 ng/ml EGF, and cultured for 7 days, as reported previously [49]. Afterwards, phase contrast images were taken with 10x objectives using an inverted microscope (Nikon Eclipse TS100, Nikon Instruments Inc.; Melville, NY). After stratification, samples were processed for H&E

staining as described above and imaged with a bright field microscope (EVOS FL Auto Cell Imaging System, Invitrogen, CA, USA).

2.13.2. Human corneal fibroblasts (HCF)—Primary human corneal fibroblasts (HCF) were also used for evaluating the recellularization potential. Cells were isolated from donated human corneoscleral rims discarded after penetrating keratoplasties performed at the Massachusetts Eye and Ear, Massachusetts, USA. Corneal tissue was processed as previously described [50], to generate corneal fibroblasts. HCF were utilized between passages 4 and 7. As with HCECs, HCF were seeded on DPC and G-DPC after soaking them in DMEM/Ham's F-12 media (Corning, Manassas, VA, USA) supplemented with 10% fetal bovine serum (FBS) for seven days. 10,000 HCF were seeded on top of 6-mm-diameter DPC and cultured using supplemented DMEM in a 37 °C, 5% CO_2 incubator under standard culture condition for 1 month. At different time points, cell viability was measured by live/dead staining. Images were taken by using a fluorescence microscope (Zeiss Axio Observer Z1, Carl Zeiss Microimaging GmbH, Jena, Germany).

2.13.3. Human corneal endothelial cells (CEC)—Telomerase immortalized human corneal endothelial cells [51] (CEC), kindly provided by Professor Ula Jurkunas, were cultured on the top of DPC and G-GPC, after soaking the tissues in Opti-MEM I with Glutamax-I media (Life Technologies Corporation, Carlsbad, CA) supplemented with 8% (v/v) FBS (Life Technologies Corporation), 5 ng/ml EGF (EMD Millipore Corporation, Temecula, CA), 0.2 mg/ml calcium chloride (Fisher Scientific Company, Fair Lawn, NJ), 0.8 mg/ml chondroitin sulfate-A (Sigma-Aldrich, St. Louis, MO), 0.25 mg/ml Gentamycin (Life Technologies Corporation), 1% (v/v) Antibiotic-Antimycotic solution (Life Technologies Corporation), and 0.1 mg/ml bovine pituitary extract (Alfa Aesar, Ward Hill, MA) for seven days. 20,000 CEC were seeded on the xenograft (Descemet's membrane side up) with the same media that was used for soaking the grafts. Media was changed every other day, and live/dead staining was performed after seven days.

2.13.4. Hybrid neuroblastoma cells (NDC)—NDC were kindly provided by May Griffith, who has used NDC as a source of neural progeny to evaluate biocompatibility on different biomaterials [52,53]. For culturing NDC, xenografts were soaked in DMEM media (Sigma-Aldrich) supplemented with 10% (v/v) FBS (Life Technologies Corporation) for seven days. 20,000 NDC were cultured directly on the top of DPC and G-DPC to evaluate the potential of the decellularized xenograft to support neural growth and live/dead staining performed at day seven.

2.14. Phenotype of HCEC after recellularization

The expression of cytokeratin 12 and mucin MUC16 by HCEC after recellularization on DPC and G-DPC was determined by fluorescence immunohistochemistry (IHC), using paraffin embedded tissue sections. The same paraffin embedding protocol was used as described above. For IHC, paraffin was removed from the tissue sections using xylene, and the samples were rehydrated in water through a graded series of alcohols (100%, 96%, 70%, 50%, and water). For antigen retrieval, tissue sections were incubated with 10 mM Sodium citrate buffer, 0.05% Tween 20 (pH 6.0) at 60 C for overnight. The sections were washed

with Tris-buffered saline (TBS) plus 0.025% Triton X-100 followed by blocking any unspecific binding sites using TBS supplemented with 10% FBS and 1% bovine serum albumin (BSA). The sections were then incubated with the primary antibodies overnight at 4 C in humidifying condition. Goat polyclonal antibody against corneal epithelial cell specific cytokeratin (anti-cytokeratin 12, sc-17101, Santa Cruz Biotechnology) and mouse monoclonal antibody against corneal mucin (anti-MUC16, clone X75; ab10029, Abcam) were used separately at dilution 1:100 and 1:300, respectively. Incubation with secondary antibodies was carried out for 1 h at room temperature. FITC-conjugated anti-goat antibody (ab150133, dilution 1:200; Abcam) and FITC-conjugated anti-mouse antibody (ab6785, dilution 1:100; Abcam) were used as secondary antibody for cytokeratin 12 and mucin, respectively. Finally, slides were mounted in VectaShield mounting medium containing DAPI (Vector Laboratories, Inc., CA, USA), and examined by an inverted fluorescent microscope (Zeiss Axio Observer Z1, Carl Zeiss Microimaging GmbH, Jena, Germany) with a 40x objective.

2.15. Ex vivo transplantation into pig eyes

The feasibility of the DPC and G-DPC to be used as a donor tissue for anterior lamellar keratoplasty (ALK) and as a carrier for Boston Keratoprosthesis Type 1 (BKPro) was tested ex vivo on pig eyes. BKPro is the most commonly used artificial cornea world-wide for severe corneal diseases that have poor prognosis with standard keratoplasty. The BKPro is a double-plated device of polymethyl methacrylate (PMMA) and titanium, which usually requires a fresh corneal graft as a carrier [50].

For ALK, host pig corneas were trephined to ~50% depth with an 8 mm Barron trephine and the anterior host tissue removed using a crescent blade. DPC and G-DPC were then trephined at 8 mm and split to half thickness to obtain the donor graft. Subsequently, donor grafts were transplanted into the previously prepared 8 mm host corneal beds using eight interrupted 10–0 nylon sutures.

A different experimental procedure was followed for the implantation of BKPro. Eleven mm diameter discs of DPC and GDPC were centrally trephined with a 3 mm trephine. The standard procedure of assembly of BKPro and donor tissue was followed [54]. Eleven mm diameter full thickness trephination of the host cornea was performed. Afterwards, BKPro-graft combination was placed in the host bed and sutured with eight interrupted 10–0 nylon sutures.

A digital microscope (Dino-Lite Edge 3.0, New Taipei City, Taiwan) was used to capture images of transplanted eyes. OCT images were obtained using a Heidelberg Spectralis HRA + OCT (Heidelberg Engineering GmbH, Heidelberg, Germany) immediately after the transplantation.

2.16. Statistical analysis

Comparisons between multiple groups were performed by ANOVA with Dunnett’s post hoc analysis. Data were log transformed before analysis to comply with the assumptions of general linear models. One-way ANOVA with Tukey post hoc was done among the groups to compare mechanical and functional characteristic properties. Differences between

densitometry values for scanned WBs were determined using ratio paired Tukey's post hoc multiple comparison tests. A value of $p < 0.05$ was considered statistically significant. n.s., *, **, ***, and **** represent p greater than 0.05, $p < 0.05$, $p < 0.01$, $p < 0.001$ and $p < 0.0001$, respectively. GraphPad Prism Software (GraphPad Software, CA, USA) was used to analyze the data.

3. Results

3.1. Evaluation of decellularization efficiency

Histological evaluation of NPC and DPC was performed (Fig. 1A). H&E staining showed that corneal epithelial cells, stromal cells, and endothelial cells were distinctly visible in the NPC. However, in the DPC, no epithelial, stromal or endothelial cells were observed. H&E also confirmed that decellularized corneas had a slightly increased thickness compared to NPC. AB staining on NPC showed the presence of GAG throughout the cornea with a higher concentration at the anterior part. Conversely, DPC showed an intense reduction of GAG that extended to the entire corneal stroma. PAS-stained carbohydrates were mainly present in the anterior two thirds of the stroma in NPC. In contrast, the carbohydrate concentration was markedly reduced in DPC. PAS staining of DPC showed the presence of an intact epithelial basement membrane and Descemet membrane.

DAPI staining revealed that 0.1% SDS solution in distilled water removed cells from all cellular layers of the porcine cornea compared to native corneas and corneas treated with dH_2O (Fig. 1B). In order to evaluate the effectiveness of the decellularization, we measured the residual number of nuclei and nuclear debris that remained on DPC after decellularization. DAPI staining indicated that the number of nuclei and area of the nuclei were significantly reduced in DPC compared to NPC ($p = 0.0001$ for both comparisons). Nuclear debris count and area measurements were consistent: DPC had significantly less nuclear debris and area of debris compared to NPC ($p = 0.0010$ and $p = 0.0006$, respectively).

WB analysis confirmed that decellularization reduced the presence of α-gal and NeuGc compared to the native cornea, $p = 0.0089$ and 0.0454, respectively (Fig. 1C). A non-significant difference in collagen type I content was observed following decellularization ($p = 0.1619$).

3.2. Transmission electron microscopy (TEM)

The structural organization of the stroma of DPC and G-DPC, including the presence of cell debris, was compared with NPC and NHC through TEM (Fig. 2). Keratocytes were visualized with low (LM) and high magnification (HM) images in the stroma. LM and HM images of mid-stroma of DPC and G-DPC confirmed the removal of keratocytes, leaving vacant spaces in the stroma. HM images of DPC and G-DPC revealed the presence of some cell debris. The ultrastructure of the extracellular matrix of the stroma and the Descemet's membrane of decellularized corneas were similar to native corneas. Highly ordered and stacked collagen lamellae were observed in all groups. In DPC and G-DPC, the collagen lamellae within the stroma were arranged parallel to each other, similar to NHC and NPC.

The collagen fibrils within the lamellae showed a similar diameter in all groups. However, the inter-fibril space varied among the different groups, with more heterogeneity in the decellularized groups, higher in G-DPC than in DPC.

3.3. Evaluation of optical properties

UV–Vis spectroscopy revealed that the final product after decellularization was transparent (Fig. 3A). However, transparency varied during the different steps of the decellularization process. DPC became transparent similar to native porcine and human corneas at the visual wavelength (400 to 700 nm). Moreover, DPC transmitted approximately 60% of the UVB light. On the other hand, G-DPC showed 40% absorption of light at the blue band with wavelengths ranging from 400 to 499 nm, and gamma irradiation caused a yellow appearance of the G-DPC (Fig. 3B). Moreover, G-DPC showed complete blocking of UV light from 250 to 400 nm. At the far visual wavelengths (around 600 nm), G-DPC were transparent to visual light, similar to NPC.

Intensity images of OCT confirmed the thickness and integrity of the corneal stroma. Intact NPC and NPC after rehydration showed the same thickness (Fig. 3C). The stroma increased after decellularization and again reduced close to NPC after gamma treatment in G-DPC. The thickness of the NPC, DPC and G-DPC was 1.27 ± 0.10 mm, 2.51 ± 0.15 mm and 1.45 ± 0.11 mm, respectively. Certain depths of the corneas appeared to be more strongly scattering due to the focusing effect of the curved cornea samples. Birefringence images of the PS-OCT, which showed additional contrast beyond the conventional intensity OCT, revealed that in NPC the differences of the refractive indices were high and were equally distributed throughout the stroma. The degree of birefringence was less prominent and more spread out in the swollen DPC compared to the NPC. After GI, the thickness was reduced, and birefringence was high throughout the cornea, which was similar to NPC.

3.4. Mechanical characterization of different porcine and human corneas

GI positively changed the mechanical properties of the decellularized xenograft, becoming stiffer than non-irradiated DPC (Fig. 4A–D). Tensile strength of G-DPC was similar to NHC ($p = 0.1495$) but significantly higher compared to DPC ($p < 0.0001$) and NPC ($p = 0.0011$) (Fig. 4A). Although, there was no significant difference in elastic modulus between NPC and DPC, G-DPC demonstrated higher elastic modulus surpassing that of NHC and NPC (Fig. 4B). Moreover, while DPC showed a higher elongation at break than NHC and NPC, elongation for G-DPC was decreased compared to NHC, NPC and DPC (Fig. 4C). We also measured the compressive modulus of different corneas until 40 N load, as the corneas were not breakable by the machine we used (Fig. 4D). G-DPC showed lower compressibility compared to the other groups as indicated by higher compressive modules.

3.5. Functional characteristic comparison among different porcine corneas

Water content of DPC was 81.3 ± 1.0%, which was significantly higher than that of G-DPC (73.6 ± 2.7%) (Fig. 4E) and closer to human corneas (78.0 ± 3.0%) [55]. G-DPC had the lowest water content although non-significantly different from human corneas. Water contents were similar for NPC and G-DPC whereas, NPC versus DPC and DPC versus G-DPC differed significantly ($p = 0.0108$ and $p = 0.0012$, respectively).

Contact angle, demonstrating the wettability of a solid surface, was investigated (Fig. 4F). Water placed on intact corneal epithelium showed significantly greater contact angle (mean, 60) than water placed directly on Bowman's layer on deepithelialized NPC (D-NPC) (mean, 48°; $p = 0.0165$). DPC had contact angle measurements similar to NPC and D-NPC. The wettability of G-DPC (mean, 101) was significantly decreased compared to DPC ($p < 0.0001$), NPC ($p < 0.0001$), and D-NPC ($p < 0.0001$).

Glucose diffusivity of DPC was significantly higher than for NPC ($p < 0.0001$) or G-DPC ($p = 0.0039$) (Fig. 4G). Glucose diffusivity of G-DPC was also significantly higher than for NPC ($p = 0.0036$).

Biodegradation was assayed *in vitro* by collagenase degradation assay measuring the relative resilience of DPC compared to G-DPC (Fig. 4H). G-DPC took two hours more to be completely digested compared to DPC and 4 h more compared to NPC (28, 26 and 24 h, respectively). After 12 h of collagenase exposure, only 25% of the residual mass was preserved for DPC, whereas, more than 50% of the residual mass was preserved for G-DPC.

3.6. Complement activation in contact with human plasma

The three activation products C3bc (Fig. 5A), C4bc (Fig. 5B), and sC5b-9 (Fig. 5C) were assessed to examine the potential effects of the differently treated porcine corneas on human complement activation using six donors. Although the C4bc values were higher in NPC than the treated corneas (DPC and G-DPC) and sC5b-9 values were higher in the G-DPC group, there were no significant differences between any of the groups.

3.7. Recellularization of DPC and G-DPC

To determine the recellularization efficiency of decellularized tissues, HCEC, HCF, CEC and NDC were seeded on the surface of DPC and G-DPC (Fig. 6A). Phase contrast microscopy images of DPC and G-DPC recellularized with HCEC demonstrated that epithelial cells were able to attach, migrate and proliferate on both surfaces when cultured with supplemented KSFM media. At confluence, upon changing media to stratification media, cells formed stratified layers of 3–4 cells on both types of decellularized cornea, as confirmed by H&E staining. Phenotypic evaluation of HCEC grown on DPC and G-DPC was carried out by immunohistochemistry (Fig. 6B). HCEC cultured on DPC and G-DPC expressed cytokeratin 12 and MUC16. Autofluorescence from decellularized tissue, especially G-DPC, compromised the picture quality. The negative control staining with only secondary antibodies is provided in the supplementary material (Fig. S1).

HCF were cultured on the surface of DPC and G-DPC and live/dead staining was performed at 15 days and one-month (Fig. 7). There were very few dead cells (red) for either tissue at each time point. Both surfaces became confluent with HCF (green) in a similar fashion. A similar result was observed for CEC, which created a monolayer of viable cells on DPC and G-DPC, as visualized with live/dead staining. A negligible numbers of dead cells on both types of xenograft were observed. NDC, a neural progenitor cell, also grew on the DPC and G-DPC, showing that both types of decellularized tissues have the potential to support neural cell growth.

3.8. Ex vivo transplantation of corneas into pig eyes

Both DPC and G-DPC were transplanted into pig eyes *ex vivo* by anterior lamellar keratoplasty and also used as a carrier for BKPro implantation (Fig. 8). The xenografts could be sutured to the host tissue similarly to human corneas. Slit lamp biomicroscopy and OCT images showed that the implant confirmed the apposition of the implanted tissue with the host cornea after ALK and BKPro. OCT images of the BKPro transplanted eye confirmed the stable assembly of BKPro into the carrier xenograft.

4. Discussion

The present study evaluates the effect of GI on sterilization of DPC for xenotransplantation. We show that GI sterilization is not deleterious for the tissue and allows retention of physiological, mechanical and optical properties needed for corneal transplantation. Since GI is an effective and accepted sterilization process of human donor corneas [56], including carriers for the BKPro [57], and porcine corneas for clinical studies [23,27], it may enable future application of DPC in humans.

Different decellularization protocols have been used in the past with mixed success [58]. Most of the protocols are based on the anionic detergent SDS. This detergent displays a high water binding capacity based on its negative charge, which causes the swelling of the target tissue, to facilitate SDS penetration and cell lysis [59]. Various concentrations of SDS were studied previously to determine an effective decellularization concentration without reducing the GAG and collagen content of decellularized corneas (DC). In many cases, SDS treatment was applied on enzyme-treated samples [60,61]. Some reports have demonstrated that a high concentration of SDS decreased the GAG content, damaged basement membrane and loosened the collagen fibrils [62,63]. We used a 0.1% SDS solution as we have previously shown that corneas treated with this concentration contained less residual nuclear debris [24]. We were able to optimize the decellularization effectiveness by changing the solvent of the solution. As we have reported here, 0.1% SDS in dH_2O removed almost all the cellular content of DPC compared to the native untreated control, without significantly disrupting the corneal extracellular matrix. Our H&E and DAPI staining confirmed the removal of the cellular component from the DPC, and the swelling of the DPC, a common consequence of decellularization [64] that could be associated with the GAG reduction observed in Alcian blue staining [65]. PAS confirmed epithelial basement membrane integrity in DPC. We also showed that the decellularization process significantly reduces the presence of α-gal and NeuGc in the DPC, without decreasing collagen type I. α-gal and NeuGc are the main pig specific xenoantigens recognized by human antibodies, and are associated with failure of porcine xenografts [66–69]. Thus, we describe a very simple and effective decellularization protocol that preserves the corneal extracellular matrix. Moreover, taking into account the inexpensiveness of the reagents used, this protocol is feasible and easily applied, and may be useful in low-income countries, where most of the corneal blind patients live [70].

Distortion of the ultra-structure of the collagen lamellae of the cornea is an undesirable effect of decellularization and sterilization processes. By TEM analysis of treated and untreated corneas, no grossly evident changes were noted in collagen fibers for DPC compared to NHC and NPC, except that the inter-fibrillar spaces were marginally larger.

This might be due to swelling as previously described by others [64]. The fact that subsequent GI reduced swelling, and partially restored the regular spacing and ordering between collagen lamellae, might be the reason for the restoration of birefringence in G-DPC back to the NPC levels. Moreover, distortion of the collagen lamellae can cause a decrease in corneal transparency. SDS treated DPC and G-DPC became transparent after soaking in glycerol. This effect of glycerol was similar to a previous report [62]. Regarding the UV transmission in GI samples, we observed that G-DPC treated with glycerol were able to completely block UV transmission. However, another research group has recently reported that GI-treated porcine corneas were equally transparent at 280 nm to 780 nm compared to non-GI corneas [71]. In this context, the lack of corneal epithelium, which protects the eye from the harmful UV radiation [72] and stromal changes that might occur after implantation may affect the UV absorption of the corneal xenograft. Thus, UV protection might be a necessary precaution for decellularized, GI-treated, porcine corneal xenografts in human patients until epithelialization of the scaffold occurs.

We also observed that gamma irradiated samples turned pale yellow. This yellowing effect was previously described in gamma irradiated human corneas and PMMA, associated with chain scission of the materials [50]. As GI can break chemical bonds and can crosslink polymers [73], fragmented collagen chains undergo a secondary crosslinking which ultimately contributes to favorable mechanical properties and resistance to enzymatic degradation, keeping the cornea compact even without the presence of a healthy corneal endothelium [74–77]. In this regard, mechanical property measurements revealed that G-DPC were the strongest showing a high tensile strength similar to NHC. The high elastic modulus of G-DPC was in the range of other types of tissues, such as cortical bone [78], which suggest that these xenografts could be applied not only as corneal or scleral substitutes but also for tissue replacement in other areas of the body. Additionally, GI modified the contact angle of the corneal surface. However, the higher contact angle showed by G-DPC was not associated with an impairment of the recellularization process by any of the cells studied in this work.

Biodegradation analysis revealed that both kinds of decellularized corneas were stable for more than 24 h, similar to native corneas, and more resistant than other type of corneal substitutes made of collagen that degrade approximately after 10 h in collagenase [79,80]. Furthermore, stromal changes induced by the decellularization and irradiation processes did not impair glucose diffusion, keeping an optimally porous structure to permit adequate distribution of solutes and nutrients [81]. Glucose diffusivity of DPC and G-DPC (2.80 ± 0.04) $\times 10^{-6}$ cm/s^2 and (2.35 ± 0.05) $\times 10^{-6}$ cm/s^2, respectively, was roughly equivalent to the diffusivity previously reported for human native corneas (2.60 ± 0.3) $\times 10^{-6}$ cm/s^2 [82].

G-DPC induced complement activation in human plasma. The level of activation was in general low and there was no significant difference in activation between treated corneas compared to native corneas. Complement activation is a crucial component in the human host response to tissue of porcine origin. Specific recognition molecules of the complement system can either bind directly or bind via natural antibodies to the tissue. Decellularization might influence immune activation, as has been observed by other research groups [83]. It should be emphasized, however, that the number of experiments were limited and further

investigation of the innate immune activation is needed, including activation of the cytokine network.

Recellularization of a decellularized xenograft is one of the most important steps to characterize them as functional corneal substitutes. Here, we observed that DPC and G-DPC both permitted the growth and migration of human corneal epithelial cells, corneal fibroblasts, corneal endothelial cells and NDC despite changes observed in the corneal extracellular matrix after decellularization and GI. GI-treated tissues had no cytotoxic effect, as shown by Gorham et al., using mouse foreskin fibroblasts [84]. Our cell study results are in the agreement with previous studies that described the capability of HCEC [60] and HCF [24] to grow on DPC treated with SDS. However, when human corneas were decellularized and recellularized with human corneal epithelial cells and fibroblasts, SDS treated corneas favored the growth of fibroblasts over epithelial cells [64]. This difference might be due to the different species used or differences on the decellularization, sterilization and recellularization protocols. Regarding fibroblastic invasion, we did not observe fibroblasts migrating inside the scaffold during the 30 days in culture. However, previous report informed about the presence of corneal fibroblasts inside the stroma of gamma irradiated xenograft after 2 months of implantation, without showing any characteristic or fibrotic response associated to myofibroblast differentiation [27].

Corneal epithelial cells grown on top of DPC and G-DPC expressed the specific epithelial corneal marker cytokeratin 12. Cytokeratin 12 is expressed in the terminally differentiated corneal epithelium predominantly in the basal cells [85], which partially correlated with the expression pattern we found in the recellularized samples, specially in G-DPC. Furthermore, epithelial cells cultured on the decellularized corneas were able to synthesize a protective mucin layer that stained with MUC16. MUC16 is a heavily glycosylated transmembrane protein expressed by the matured apical and subapical flattened cells of the human corneal epithelium. It is localized on the tips of the surface microplicae, providing an anti-adherent barrier to the epithelial layer, which is crucial for the homeostasis of the epithelium [86]. It was shown previously that immortalized human corneal cells also express MUC16 [87], characteristically in the epithelial surface microplicae [88]. We found the same expression pattern in the stratified epithelium grown on the decellularized corneas. Both types of decellularized xenografts also supported corneal endothelial cell growth. It was previously shown that SDS treated porcine cornea facilitated CEC growth in-vitro [89]. NDC were used to evaluate the potential for neural growth in xenografts. NDC are a hybrid created by fusion of the two cell types; rodent dorsal root ganglion and neuroblastoma cells [90], and have grown as mature sensory neurons. They can extend neurites and produce substance P [90,91]. NDC were able to adhere and proliferate on both types of decellularized xenografts, suggesting the potential of the graft to facilitate neural growth.

Our *ex vivo* work placing G-DPC explants either as a lamellar keratoplasty or as a carrier for the BKPro was preliminary but showed the feasibility of using G-DPC as corneal substitute. However, to show convincing evidence for the beneficial effect of G-DPC in clinical practice, we need to perform long-term *in vivo* studies using optimal animal models. The animal model used should be representative of humans in terms of biointegration and biocompatibility. In this regard, the only model that mimics the human response to

xenografts, including the presence of natural antibodies against alpha gal epitope, is Old World primates [92]. Choi et al. performed one of the very few studies where Old World primates were used to evaluate decellularized non-irradiated xenografts. Decellularized and fresh porcine corneas were compared by transplanting into rhesus macaques. Despite the use of immune suppression, half of the untreated corneas developed rejection, whereas 80% of the DPCs remained transparent for more than 6 months [15].

5. Conclusion

In conclusion, we evaluated the effect of sterilizing decellularized porcine corneas for transplantation using gamma irradiation. According to our results, this sterilization method is not deleterious for corneal tissue and allows retention of physiological, mechanical and optical properties required for corneal transplantation. Additionally, we observed that the applied decellularization protocol efficiently removed the majority of the antigenic elements of porcine corneas. The use of this decellularization protocol combined with gamma radiation sterilization is promising as an alternative to corneal allograft in the treatment of human patients with corneal blindness.

Supplementary Material

Refer to Web version on PubMed Central for supplementary material.

Acknowledgement

This paper was supported by Boston-KPro research fund: Boston, MA, USA; and NIH National Eye Institute: Bethesda, MD, USA; Core Grant P30EY003790, and an unrestricted grant to the Department of Ophthalmology, Harvard Medical School, by Research to Prevent Blindness, NY, NY. Financial support was also obtained from The Odd Fellow Foundation: Oslo, Norway; and The Simon Fougner Hartmann Family: Dragør, Denmark Fund. PCH was supported by the Croucher Fellowship. MG and JK acknowledge the support of HK ITC grant reference: ITS/195/14FP. Access to the PS-OCT instrumentation and processing tools was provided by the Center for Biomedical OCT Research and Translation, which is supported by the Nationals Institutes of Health (grant P41EB-015903). The authors gratefully acknowledge support from the Department of Biological Engineering of MIT for gamma irradiation and Oscar Morales (Schepens Eye Research Institute) for assisting with the OCT *ex vivo* work. We also appreciate the aid of Bianai Fan and Philip Seifert (Schepens Eye Research Institute) in the light and electron microscopy studies, respectively.

References

[1]. World Health Organization (WHO). Prevention of Blindness and Visual Impairment. http://www.who.int/blindness/en. (Accessed 28 July 2017).

[2]. Brunette I, Roberts CJ, Vidal F, Harissi-Dagher M, Lachaine J, Sheardown H, Durr GM, Proulx S, Griffith M, Alternatives to eye bank native tissue for corneal stromal replacement, Progr. Retinal Eye Res 59 (2017) 97–130.

[3]. Oliva MS, Schottman T, Gulati M, Turning the tide of corneal blindness, Indian J. Ophthalmol 60 (5) (2012) 423–427. [PubMed: 22944753]

[4]. Gain P, Jullienne R, He Z, Aldossary M, Acquart S, Cognasse F, Thuret G, Global survey of corneal transplantation and eye banking, JAMA Ophthalmol. 134 (2) (2016) 167–173. [PubMed: 26633035]

[5]. Wong KH, Kam KW, Chen LJ, Young AL, Corneal blindness and current major treatment concern-graft scarcity, Int. J. Ophthalmol 10 (7) (2017) 1154–1162. [PubMed: 28730122]

[6]. Panda A, Vanathi M, Kumar A, Dash Y, Priya S, Corneal graft rejection, Surv. Ophthalmol 52 (4) (2007) 375–396. [PubMed: 17574064]

[7]. Cruzat A, Tauber A, Shukla A, Paschalis EI, Pineda R, Dohlman CH, Low-cost and readily available tissue carriers for the Boston keratoprosthesis: a review of possibilities, J. Ophthalmol 2013 (2013) 686587.

[8]. Kissam RS, Ceratoplastice in man, New York Med. J 2 (1844). 281 281.

[9]. ARTIFICIAL CORNEA, The Lancet 138(3555) (1891) 886.

[10]. Soomsawasdi B, Romayanonda N, Bhadrakom S, Hetero-keratoplasy using gibbon donor corneae, Asia Pacific Acad. Ophthalmol 2 (1964) 251–261.

[11]. Durrani KM, Kirmani TH, Hassan MM, Rizvi SM, Tanner JC, Vandeput JJ, Penetrating keratoplasty with purified bovine collagen: report of a coordinated trial on fifteen human cases, Ann. Ophthalmol 6 (6) (1974) 639–646. [PubMed: 4599525]

[12]. De Ocampo G, Sunga R, De La Cruz-Estrella C, The use of chicken and monkey cornea for human corneal grafting, Acta Med. Philipp 16 (1959) 55–64. [PubMed: 13884444]

[13]. Haq M, Fish cornea for grafting, Br. Med. J 2 (5815) (1972) 712–713.

[14]. Larkin DF, Williams KA, The host response in experimental corneal xenotransplantation, Eye 9 (Pt 2) (1995) 254–260. [PubMed: 7556727]

[15]. Choi HJ, Kim MK, Lee HJ, Ko JH, Jeong SH, Lee JI, Oh BC, Kang HJ, Wee WR, Efficacy of pig-to-rhesus lamellar corneal xenotransplantation, Invest Ophthalmol. Vis. Sci 52 (9) (2011) 6643–6650. [PubMed: 21743020]

[16]. Boneva RS, Folks TM, Chapman LE, Infectious disease issues in xenotransplantation, Clin. Microbiol. Rev 14 (1) (2001) 1–14. [PubMed: 11148000]

[17]. Badylak SF, Xenogeneic extracellular matrix as a scaffold for tissue reconstruction, Transpl. Immunol 12 (3–4) (2004) 367–377. [PubMed: 15157928]

[18]. Cooper DK, Gollackner B, Sachs DH, Will the pig solve the transplantation backlog?, Ann Rev. Med 53 (2002) 133–147. [PubMed: 11818467]

[19]. Lee HI, Kim MK, Ko JH, Lee HJ, Lee JH, Wee WR, The characteristics of porcine cornea as a xenograft, J. Korean Ophthalmol. Soc 47 (12) (2006) 2020–2029.

[20]. Sharifi R, Yang Y, Adibnia Y, Dohlman CH, Chodosh J, Gonzalez-Andrades M, Finding an optimal corneal xenograft using comparative analysis of corneal matrix proteins across species, Sci. Rep 9 (1) (2019) 1876. [PubMed: 30755666]

[21]. Hashimoto Y, Funamoto S, Sasaki S, Negishi J, Honda T, Hattori S, Nam K, Kimura T, Mochizuki M, Kobayashi H, Kishida A, Corneal regeneration by deep anterior lamellar keratoplasty (DALK) using decellularized corneal matrix, PLoS ONE 10 (7) (2015) e0131989.

[22]. Gonzalez-Andrades M, Carriel V, Rivera-Izquierdo M, Garzon I, Gonzalez-Andrades E, Medialdea S, Alaminos M, Campos A, Effects of detergent-based protocols on decellularization of corneas with sclerocorneal limbus. evaluation of regional differences, Transl. Vis. Sci. Technol 4 (2) (2015) 13.

[23]. Zhang MC, Liu X, Jin Y, Jiang DL, Wei XS, Xie HT, Lamellar keratoplasty treatment of fungal corneal ulcers with acellular porcine corneal stroma, Am. J. Transplant 15 (4) (2015) 1068–1075. [PubMed: 25762108]

[24]. Gonzalez-Andrades M, de J. la Cruz Cardona AM. Ionescu A. Campos M. del Mar Perez M. Alaminos, Generation of bioengineered corneas with decellularized xenografts and human keratocytes, Invest. Ophthalmol. Vis. Sci 52 (1) (2011) 215–222. [PubMed: 20739475]

[25]. Lynch AP, Ahearne M, Strategies for developing decellularized corneal scaffolds, Exp Eye Res. 108 (2013) 42–47. [PubMed: 23287438]

[26]. Huang YH, Tseng FW, Chang WH, Peng IC, Hsieh DJ, Wu SW, Yeh ML, Preparation of acellular scaffold for corneal tissue engineering by supercritical carbon dioxide extraction technology, Acta Biomater. 58 (2017) 238–243. [PubMed: 28579539]

[27]. Shi Y, Bikkuzin T, Song Z, Jin X, Jin H, Li X, Zhang H, Comprehensive evaluation of decellularized porcine corneal after clinical transplantation, Xenotransplantation 24 (6) (2017).

[28]. Miekka SI, Forng RY, Rohwer RG, MacAuley C, Stafford RE, Flack SL, MacPhee M, Kent RS, Drohan WN, Inactivation of viral and prion pathogens by γ-irradiation under conditions that maintain the integrity of human albumin, Vox Sang. 84 (1) (2003) 36–44. [PubMed: 12542732]

[29]. Singh R, Singh D, Singh A, Radiation sterilization of tissue allografts: a review, World J. Radiol 8 (4) (2016) 355–369. [PubMed: 27158422]

[30]. Wee SW, Choi SU, Kim JC, Deep anterior lamellar keratoplasty using irradiated acellular cornea with amniotic membrane transplantation for intractable ocular surface diseases, Korean J. Ophthalmol 29 (2) (2015) 79–85. [PubMed: 25829823]

[31]. Stevenson W, Cheng SF, Emami-Naeini P, Hua J, Paschalis EI, Dana R, Saban DR, Gamma-irradiation reduces the allogenicity of donor corneas, Invest Ophthalmol. Vis. Sci 53 (11) (2012) 7151–7158. [PubMed: 22991417]

[32]. Utine CA, Tzu JH, Akpek EK, Lamellar keratoplasty using gamma-irradiated corneal lenticules, Am. J. Ophthalmol 151 (1) (2011). pp. 170–174 e1. [PubMed: 21145036]

[33]. Yuan C, Bothun ED, Hardten DR, Tolar J, McLoon LK, A novel explanation of corneal clouding in a bone marrow transplant-treated patient with Hurler syndrome, Exp. Eye Res 148 (2016) 83–89. [PubMed: 27235795]

[34]. O'Rahilly R, Meyer DB, The periodic acid-Schiffreaction in the cornea of the developing chick, Z. Anat. Entwicklungsgesch 121 (1960) 351–368. [PubMed: 14428113]

[35]. IAEA: Good radiation practice (GRP). In: IAEA (ed) Guidelines for industrial radiation sterilization of disposable medical products (cobalt-60 gamma irradiation). IAEA, Vienna, Austria, 1990.

[36]. Seifert P, Modified Hiraoka TEM grid staining apparatus and technique using 3D printed materials and gadolinium triacetate tetrahydrate, a nonradioactive uranyl acetate substitute, J. Histotechnol 40 (4) (2017) 130–135. [PubMed: 31105361]

[37]. Lo WC, Villiger M, Golberg A, Broelsch GF, Khan S, Lian CG, Austen WG Jr., Yarmush M, Bouma BE, Longitudinal, 3D imaging of collagen remodeling in murine hypertrophic scars in vivo using polarization-sensitive optical frequency domain imaging, J. Invest. Dermatol 136 (1) (2016) 84–92. [PubMed: 26763427]

[38]. Villiger M, Otsuka K, Karanasos A, Doradla P, Ren J, Lippok N, Shishkov M, Daemen J, Diletti R, van Geuns RJ, Zijlstra F, van Soest G, Libby P, Regar E, Nadkarni SK, Bouma BE, Coronary plaque microstructure and composition modify optical polarization: a new endogenous contrast mechanism for optical frequency domain imaging, JACC CardiovascImag. (2017).

[39]. Gotzinger E, Pircher M, Sticker M, Fercher AF, Hitzenberger CK, Measurement and imaging of birefringent properties of the human cornea with phase-resolved, polarization-sensitive optical coherence tomography, J. Biomed. Opt 9 (1) (2004) 94–102. [PubMed: 14715060]

[40]. Villiger M, Zhang EZ, Nadkarni SK, Oh WY, Vakoc BJ, Bouma BE, Spectral binning for mitigation of polarization mode dispersion artifacts in catheter-based optical frequency domain imaging, Opt Exp. 21 (14) (2013) 16353–16369.

[41]. Nara S, Chameettachal S, Midha S, Singh H, Tandon R, Mohanty S, Ghosh S, Strategies for faster detachment of corneal cell sheet using micropatterned thermoresponsive matrices, J. Mater. Chem. B 3 (20) (2015) 4155–4169.

[42]. Myung D, Derr K, Huie P, Noolandi J, Ta KP, Ta CN, Glucose permeability of human, bovine, and porcine corneas in vitro, Ophthal. Res 38 (3) (2006) 158–163.

[43]. Islam MM, Ravichandran R, Olsen D, Ljunggren MK, Fagerholm P, Lee CJ, Griffith M, Phopase J, Self-assembled collagen-like-peptide implants as alternatives to human donor corneal transplantation, RSC Adv. 6 (61) (2016) 55745–55749.

[44]. Mollnes TE, Brekke OL, Fung M, Fure H, Christiansen D, Bergseth G, Videm V, Lappegard KT, Kohl J, Lambris JD, Essential role of the C5a receptor in E coli-induced oxidative burst and phagocytosis revealed by a novel lepirudin-based human whole blood model of inflammation, Blood 100 (5) (2002) 1869–1877. [PubMed: 12176911]

[45]. Bergseth G, Ludviksen JK, Kirschfink M, Giclas PC, Nilsson B, Mollnes TE, An international serum standard for application in assays to detect human complement activation products, Mol. Immunol 56 (3) (2013) 232–239. [PubMed: 23787367]

[46]. Orrem HL, Nilsson PH, Pischke SE, Grindheim G, Garred P, Seljeflot I, Husebye T, Aukrust P, Yndestad A, Andersen GO, Barratt-Due A, Mollnes TE, Acute heart failure following myocardial infarction: complement activation correlates with the severity of heart failure in

patients developing cardiogenic shock, ESC Heart Fail 5 (3) (2018) 292–301. [PubMed: 29424484]

[47]. Mirazul Islam M, Cėpla V, He C, Edin J, Rakickas T, Kobuch K, Ruželė Ž, Bruce Jackson W, Rafat M, Lohmann CP, Valiokas R, Griffith M, Functional fabrication of recombinant human collagen–phosphorylcholine hydrogels for regenerative medicine applications, Acta Biomater. 12 (2015) 70–80. [PubMed: 25448347]

[48]. Araki-Sasaki K, Ohashi Y, Sasabe T, Hayashi K, Watanabe H, Tano Y, Handa H, An SV40-immortalized human corneal epithelial cell line and its characterization, Invest. Ophthalmol. Vis. Sci 36 (3) (1995) 614–621. [PubMed: 7534282]

[49]. Gonzalez-Andrades M, Alonso-Pastor L, Mauris J, Cruzat A, Dohlman CH, Argueso P, Establishment of a novel in vitro model of stratified epithelial wound healing with barrier function, Sci. Rep 6 (2016) 19395.

[50]. Gonzalez-Andrades M, Sharifi R, Islam MM, Divoux T, Haist M, Paschalis EI, Gelfand L, Mamodaly S, Di Cecilia L, Cruzat A, Ulm FJ, Chodosh J, Delori F, Dohlman CH, Improving the practicality and safety of artificial corneas: preassembly and gamma-rays sterilization of the Boston Keratoprosthesis, Ocul. Surf 16 (3) (2018) 322–330. [PubMed: 29627599]

[51]. Schmedt T, Chen Y, Nguyen TT, Li S, Bonanno JA, Jurkunas UV, Telomerase immortalization of human corneal endothelial cells yields functional hexagonal monolayers, PLoS ONE 7 (12) (2012) e51427.

[52]. Hackett JM, Ferguson C, Dare E, McLaughlin CR, Griffith M, Optimal neural differentiation and extension of hybrid neuroblastoma cells (NDC) for nerve-target evaluations using a multifactorial approach, Toxicol. In Vitro 24 (2) (2010) 567–577. [PubMed: 19883748]

[53]. Koh LB, Islam MM, Mitra D, Noel CW, Merrett K, Odorcic S, Fagerholm P, Jackson WB, Liedberg B, Phopase J, Griffith M, Epoxy cross-linked collagen and collagen-laminin peptide hydrogels as corneal substitutes, J. Funct. Biomater 4 (3) (2013) 162–177. [PubMed: 24956085]

[54]. Todani A, Ciolino JB, Ament JD, Colby KA, Pineda R, Belin MW, Aquavella JV, Chodosh J, Dohlman CH, Titanium back plate for a PMMA keratoprosthesis: clinical outcomes, Graefes Arch. Clin. Exp. Ophthalmol 249 (10) (2011) 1515–1518. [PubMed: 21519940]

[55]. Rafat M, Li F, Fagerholm P, Lagali NS, Watsky MA, Munger R, Matsuura T, Griffith M, PEG-stabilized carbodiimide crosslinked collagen-chitosan hydrogels for corneal tissue engineering, Biomaterials 29 (29) (2008) 3960–3972. [PubMed: 18639928]

[56]. Daoud YJ, Smith R, Smith T, Akpek EK, Ward DE, Stark WJ, The intraoperative impression and postoperative outcomes of gamma-irradiated corneas in corneal and glaucoma patch surgery, Cornea 30 (12) (2011) 1387–1391. [PubMed: 21993467]

[57]. Fadlallah A, Atallah M, Cherfan G, Awwad ST, Syed ZA, Melki SA, Gamma-irradiated corneas as carriers for the Boston type 1 keratoprosthesis: advantages and outcomes in a surgical mission setting, Cornea 33 (3) (2014) 235–239. [PubMed: 24457451]

[58]. Kim MK, Hara H, Current status of corneal xenotransplantation, Int. J. Surg 23 (Pt B) (2015) 255–260. [PubMed: 26231995]

[59]. Du L, Wu X, Pang K, Yang Y, Histological evaluation and biomechanical characterisation of an acellular porcine cornea scaffold, Br. J. Ophthalmol 95 (3) (2011) 410–414. [PubMed: 20956275]

[60]. Yoeruek E, Bayyoud T, Maurus C, Hofmann J, Spitzer MS, Bartz-Schmidt KU, Szurman P, Decellularization of porcine corneas and repopulation with human corneal cells for tissue-engineered xenografts, Acta Ophthalmol. 90 (2) (2012) e125–e131. [PubMed: 22136333]

[61]. Yoeruek E, Bayyoud T, Maurus C, Hofmann J, Spitzer MS, Bartz-Schmidt KU, Szurman P, Reconstruction of corneal stroma with decellularized porcine xenografts in a rabbit model, Acta Ophthalmol. 90 (3) (2012) e206–e210. [PubMed: 22136520]

[62]. Pang K, Du L, Wu X, A rabbit anterior cornea replacement derived from acellular porcine cornea matrix, epithelial cells and keratocytes, Biomaterials 31 (28) (2010) 7257–7265. [PubMed: 20598368]

[63]. Sasaki S, Funamoto S, Hashimoto Y, Kimura T, Honda T, Hattori S, Kobayashi H, Kishida A, Mochizuki M, In vivo evaluation of a novel scaffold for artificial corneas prepared by using ultrahigh hydrostatic pressure to decellularize porcine corneas, Mol. Vis 15 (2009) 2022–2028. [PubMed: 19844587]

[64]. Shafiq MA, Gemeinhart RA, Yue BY, Djalilian AR, Decellularized human cornea for reconstructing the corneal epithelium and anterior stroma, Tissue Eng. Part C Methods 18 (5) (2012) 340–348. [PubMed: 22082039]

[65]. Mendoza-Novelo B, Avila EE, Cauich-Rodriguez JV, Jorge-Herrero E, Rojo FJ, Guinea GV, Mata-Mata JL, Decellularization of pericardial tissue and its impact on tensile viscoelasticity and glycosaminoglycan content, Acta Biomater. 7 (3) (2011) 1241–1248. [PubMed: 21094703]

[66]. Cooper DK, Good AH, Koren E, Oriol R, Malcolm AJ, Ippolito RM, Neethling FA, Ye Y, Romano E, Zuhdi N, Identification of alpha-galactosyl and other carbohydrate epitopes that are bound by human anti-pig antibodies: relevance to discordant xenografting in man, Transpl. Immunol 1 (3) (1993) 198–205. [PubMed: 7521740]

[67]. Lee HI, Kim MK, Oh JY, Ko JH, Lee HJ, Wee WR, Lee JH, Gal alpha(1–3)gal expression of the cornea in vitro, in vivo and in xenotransplantation, Xenotransplantation 14 (6) (2007) 612–618. [PubMed: 17991149]

[68]. Irie A, Koyama S, Kozutsumi Y, Kawasaki T, Suzuki A, The molecular basis for the absence of N-glycolylneuraminic acid in humans, J. Biol. Chem 273 (25) (1998) 15866–15871. [PubMed: 9624188]

[69]. Zhu A, Hurst R, Anti-N-glycolylneuraminic acid antibodies identified in healthy human serum, Xenotransplantation 9 (6) (2002) 376–381. [PubMed: 12371933]

[70]. Pascolini D, Mariotti SP, Global estimates of visual impairment: 2010, Br. J. Ophthalmol 96 (5) (2012) 614–618. [PubMed: 22133988]

[71]. Lin Y, Zheng Q, Hua S, Meng Y, Chen W, Wang Y, Cross-linked decellularized porcine corneal graft for treating fungal keratitis, Sci. Rep 7 (1) (2017) 9955. [PubMed: 28855517]

[72]. Bashir H, Seykora JT, Lee V, Invisible shield: review of the corneal epithelium as a barrier to UV radiation pathogens, and other environmental stimuli, J. Ophthalmic Vis. Res 12 (3) (2017) 305–311. [PubMed: 28791065]

[73]. Cheung DT, Perelman N, Tong D, Nimni ME, The effect of c-irradiation on collagen molecules, isolated a-chains, and crosslinked native fibers, J. Biomed. Mater. Res 24 (5) (1990) 581–589. [PubMed: 2324128]

[74]. Yoshida J, Heflin T, Zambrano A, Pan Q, Meng H, Wang J, Stark WJ, Daoud YJ, Gamma-irradiated sterile cornea for use in corneal transplants in a rabbit model, Middle East Afr. J. Ophthalmol 22 (3) (2015) 346–351. [PubMed: 26180475]

[75]. Leontiou I, Matthopoulos DP, Tzaphlidou M, Glaros D, The effect of gamma irradiation on collagen fibril structure, Micron 24 (1) (1993) 13–16.

[76]. Bailey AJ, Rhodes DN, Cater CW, Irradiation-induced crosslinking of collagen, Radiat. Res 22 (4) (1964) 606–621. [PubMed: 14201872]

[77]. Tzaphlidou M, Leontiou I, Glaros D, The effect of gamma irradiation on the organization of mouse skin collagen fibrils. The positive staining pattern, Micron. Microscop. Acta 22 (3) (1991) 207–212.

[78]. Lai YS, Chen WC, Huang CH, Cheng CK, Chan KK, Chang TK, The effect of graft strength on knee laxity and graft in-situ forces after posterior cruciate ligament reconstruction, PLoS ONE 10 (5) (2015) e0127293.

[79]. Merrett K, Liu W, Mitra D, Camm KD, McLaughlin CR, Liu Y, Watsky MA, Li F, Griffith M, Fogg DE, Synthetic neoglycopolymer-recombinant human collagen hybrids as biomimetic crosslinking agents in corneal tissue engineering, Biomaterials 30 (29) (2009) 5403–5408. [PubMed: 19576630]

[80]. Liu W, Merrett K, Griffith M, Fagerholm P, Dravida S, Heyne B, Scaiano JC, Watsky MA, Shinozaki N, Lagali N, Munger R, Li F, Recombinant human collagen for tissue engineered corneal substitutes, Biomaterials 29 (9) (2008) 1147–1158. [PubMed: 18076983]

[81]. Sweeney DF, Xie RZ, O'Leary DJ, Vannas A, Odell R, Schindhelm K, Cheng HY, Steele JG, Holden BA, Nutritional requirements of the corneal epithelium and anterior stroma: clinical findings, Invest Ophthalmol. Vis. Sci 39 (2) (1998) 284–291. [PubMed: 9477984]

[82]. McCarey BE, Schmidt FH, Modeling glucose distribution in the cornea, Curr. Eye Res 9 (11) (1990) 1025–1039. [PubMed: 2095317]

[83]. Bastian F, Stelzmuller ME, Kratochwill K, Kasimir MT, Simon P, Weigel G, IgG deposition and activation of the classical complement pathway involvement in the activation of human granulocytes by decellularized porcine heart valve tissue, Biomaterials 29 (12) (2008) 1824–1832. [PubMed: 18258297]

[84]. Gorham SD, Srivastava S, French DA, Scott R, The effect of gamma-ray and ethylene oxide sterilization on collagen-based wound-repair materials, J. Mater. Sci. - Mater. Med 4 (1) (1993) 40–49.

[85]. Tanifuji-Terai N, Terai K, Hayashi Y, Chikama T, Kao WW, Expression of keratin 12 and maturation of corneal epithelium during development and postnatal growth, Invest Ophthalmol. Vis. Sci 47 (2) (2006) 545–551. [PubMed: 16431949]

[86]. Shirai K, Okada Y, Cheon DJ, Miyajima M, Behringer RR, Yamanaka O, Saika S, Effects of the loss of conjunctival Muc16 on corneal epithelium and stroma in mice, Invest Ophthalmol. Vis. Sci 55 (6) (2014) 3626–3637. [PubMed: 24812549]

[87]. Gipson IK, Spurr-Michaud S, Argueso P, Tisdale A, Ng TF, Russo CL, Mucin gene expression in immortalized human corneal-limbal and conjunctival epithelial cell lines, Invest Ophthalmol. Vis. Sci 44 (6) (2003) 2496–2506. [PubMed: 12766048]

[88]. Gipson IK, Spurr-Michaud S, Tisdale A, Menon BB, Comparison of the transmembrane mucins MUC1 and MUC16 in epithelial barrier function, PLoS ONE 9 (6) (2014) e100393.

[89]. Ju C, Gao L, Wu X, Pang K, A human corneal endothelium equivalent constructed with acellular porcine corneal matrix, Indian J. Med. Res 135 (6) (2012) 887–894. [PubMed: 22825608]

[90]. Wood JN, Bevan SJ, Coote PR, Dunn PM, Harmar A, Hogan P, Latchman DS, Morrison C, Rougon G, Theveniau M, et al., Novel cell lines display properties of nociceptive sensory neurons, Proc. Biol. Sci 241 (1302) (1990) 187–194. [PubMed: 1979443]

[91]. Newman KD, McLaughlin CR, Carlsson D, Li F, Liu Y, Griffith M, Bioactive hydrogel-filament scaffolds for nerve repair and regeneration, Int. J. Artif. Organs 29 (11) (2006) 1082–1091. [PubMed: 17160966]

[92]. Huai G, Qi P, Yang H, Wang Y, Characteristics of alpha-Gal epitope, anti-Gal antibody, alpha1,3 galactosyltransferase and its clinical exploitation (review), Int. J. Mol. Med 37 (1) (2016) 11–20. [PubMed: 26531137]

Statement of significance

In the context of bringing decellularized porcine corneas (DPC) into clinical reality, effective tissue sterilization is a crucial step. Gamma irradiation (GI) is an established and effective sterilization method for xenografts intended for human transplantation. However, little is known about the effect of GI sterilization of decellularized corneas, despite recent application in clinical studies. Here, we evaluate the effect of GI on the ultrastructure, optical, mechanical and biological properties of DPC in preparation for clinical translation. Our results suggest that GI is not deleterious for the tissue and allows retention of physiological, mechanical and optical properties which are critical for the success of corneal transplantation.

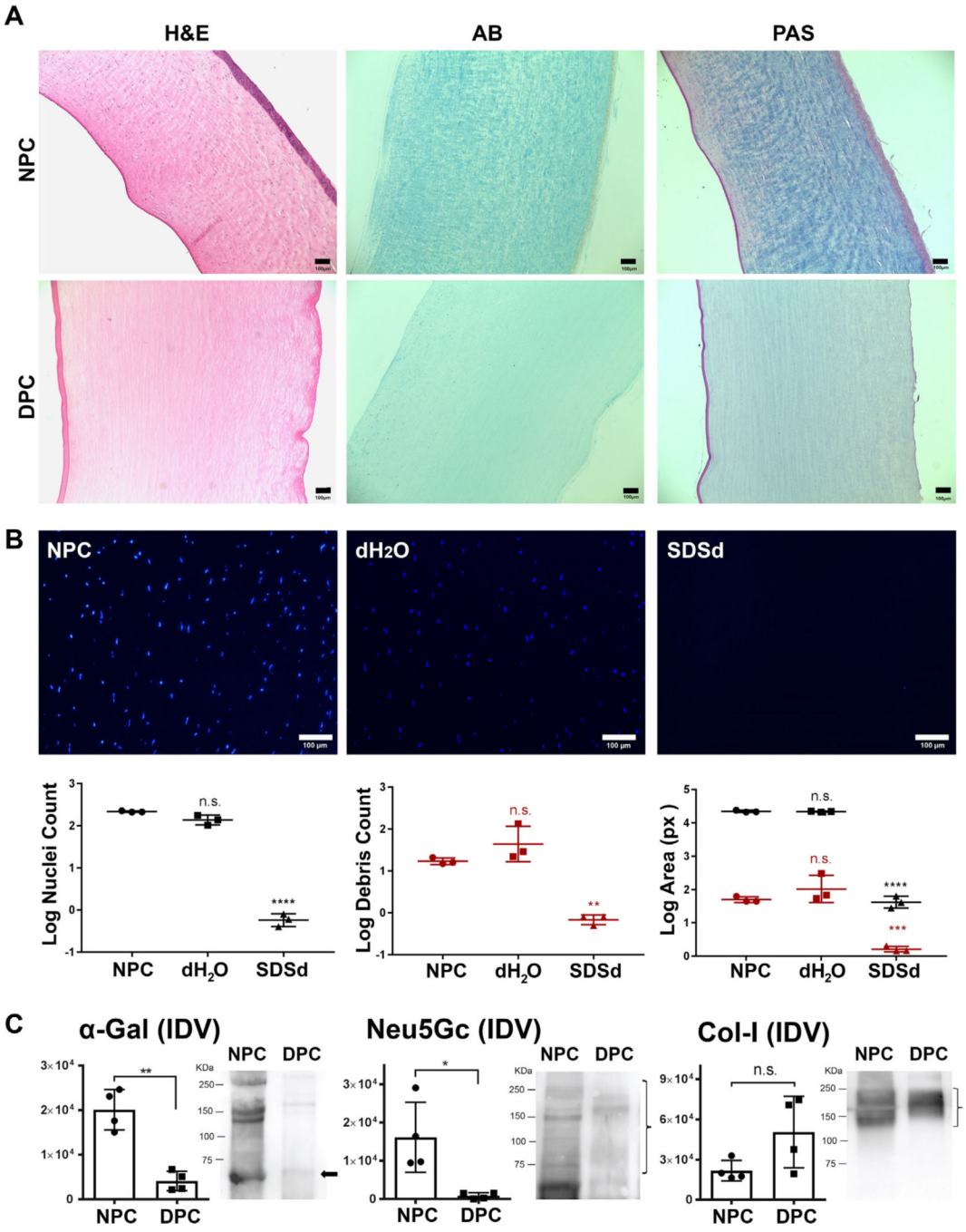

Fig. 1.

Assessment of decellularization efficiency. (A) Histological evaluation by staining with Hematoxylin and Eosin (H&E), Alcian Blue (AB) and Periodic Acid Schiff (PAS) on decellularized porcine cornea (DPC) compared with native porcine cornea (NPC). (B) Confirmation of decellularization by DAPI staining of nuclei and nuclear debris within NPC, corneas treated with distilled water (dH_2O) and corneas treated with SDS in distilled water (SDSd). Graphs represent the nuclei (black color) and nuclear debris (red color) count and area covered by them. The results were reported as the mean ± S.D. Scale bars: 100 μm. (C)

Specific detection of α-gal, Neu5Gc and collagen-I by Western Blot (WB) in NPC and DPC. The integrated density value (IDV) of each band was measured. Bar charts represent the calculated intensity of corresponding proteins using ImageJ densitometry. The results were reported as the mean ± S.D. from four independent corneas. Representative images of the WB are shown on the right (bands of interest are marked with arrow or bracket).

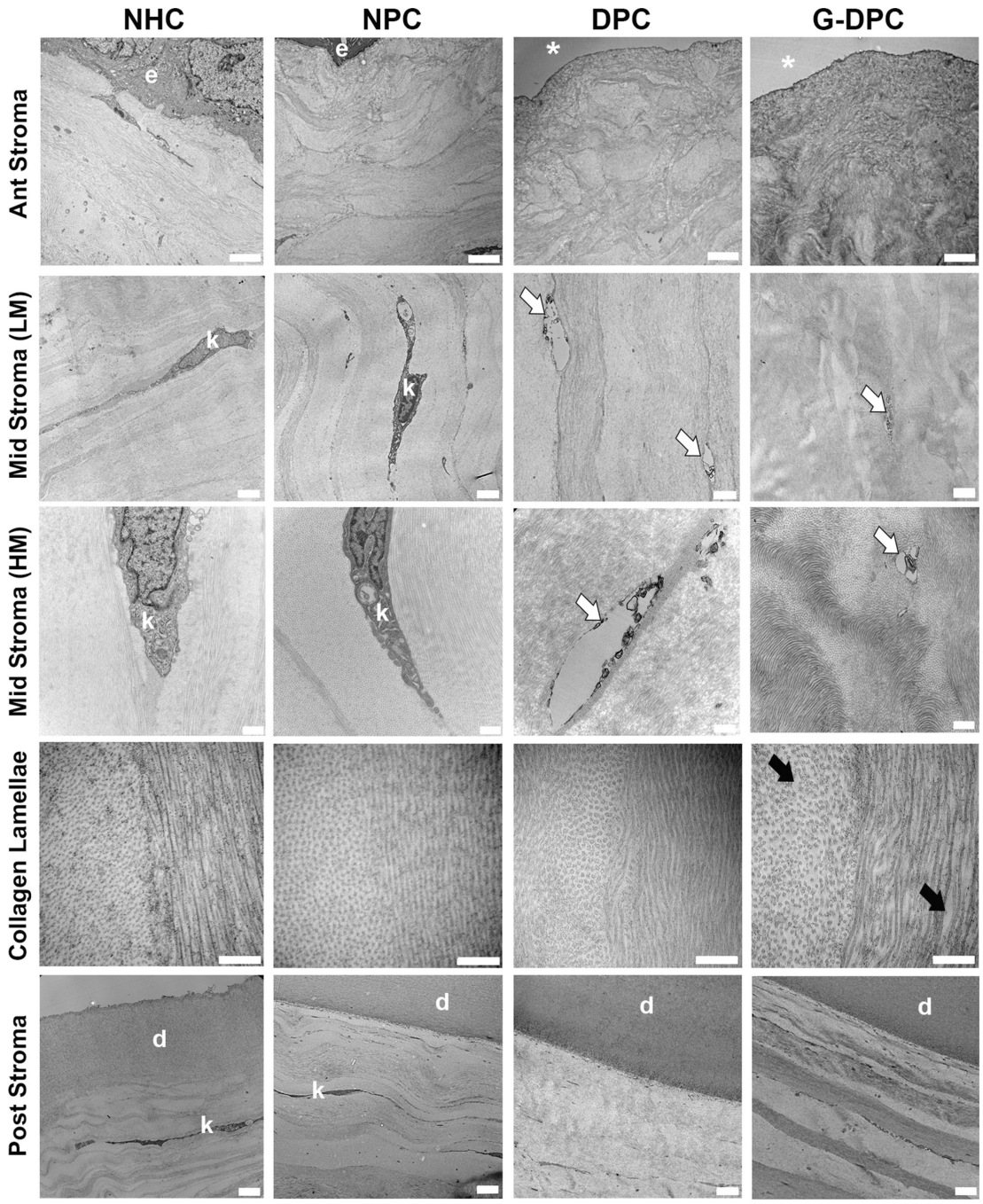

Fig. 2.

Transmission electron microscopy (TEM) micrographs of native porcine corneas (NPC), decellularized porcine cornea (DPC) and gamma irradiated decellularized porcine cornea (G-DPC); compared with native human cornea (NHC) at different layers of the cornea and at different magnifications (LM, low magnifications and HM, high magnification). e: epithelium; *: absence of epithelium; k: keratocyte; white arrows: presence of debris after decellularization; black arrows: increased space between collagen fibrils after gamma

irradiation; d: Descemet's membrane. Scale bars: for 1st, 2nd and 5th row, 2 μm; for 3rd row, 500 nm; for 4th row, 100 nm.

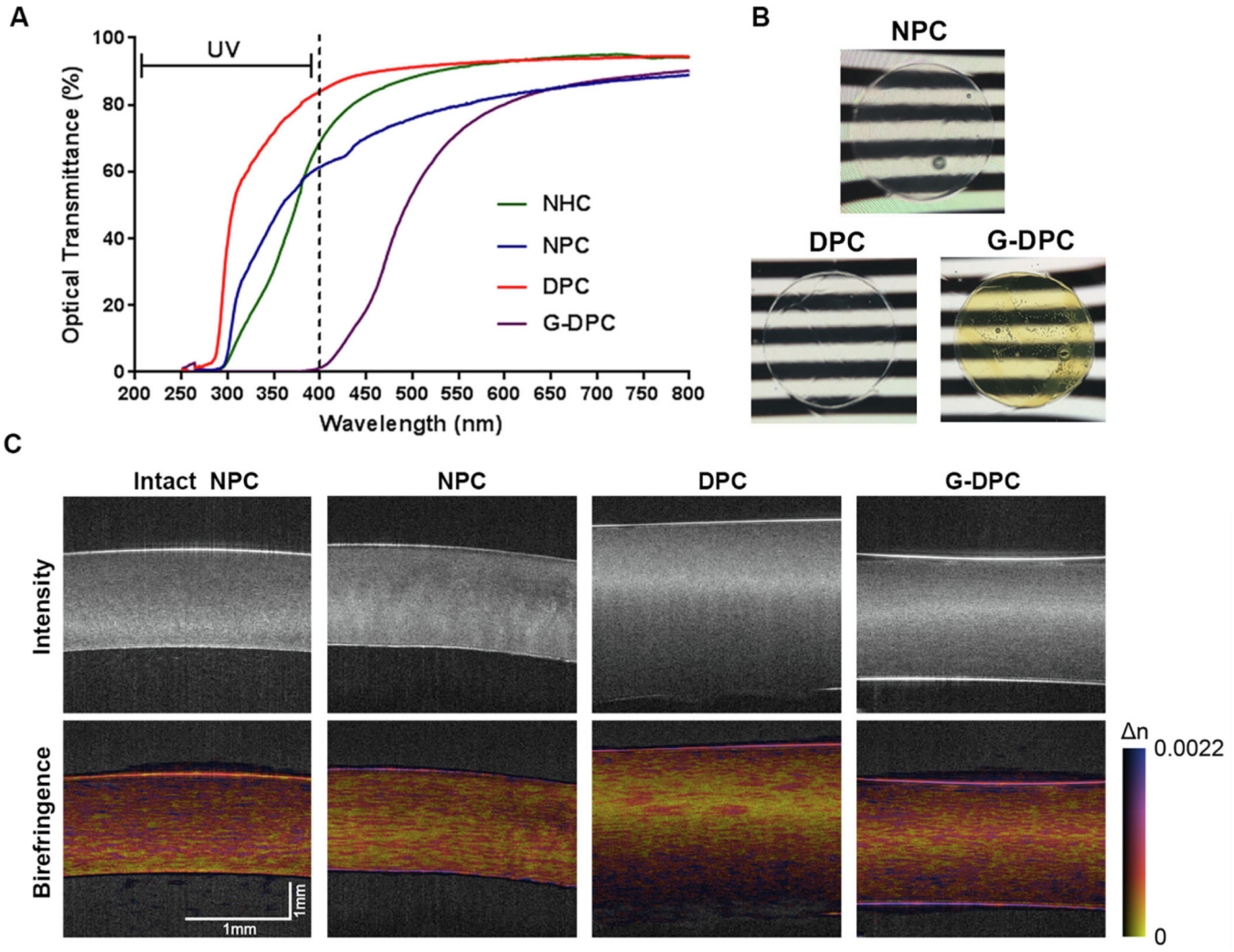

Fig. 3.

Optical evaluation of decellularized and gamma irradiated porcine corneas. (A) Light transmission through the native human cornea (NHC), native porcine cornea (NPC), decellularized porcine cornea (DPC) and gamma irradiated decellularized porcine cornea (G-DPC); from UV to visual wavelengths. (B) Macro pictures of porcine corneas after different treatments placed on a black-white stripe pattern projected on a self-illuminated screen. (C) Intensity (conventional OCT) and birefringence (PS-OCT) images of the intact porcine cornea before extraction from the eye globe (intact NPC), together with native and treated corneas. The color bar of the birefringence images displays a range of refractive index contrast from 0 to 0.0022. The birefringence values were only plotted in areas with a sufficiently high degree of polarization.

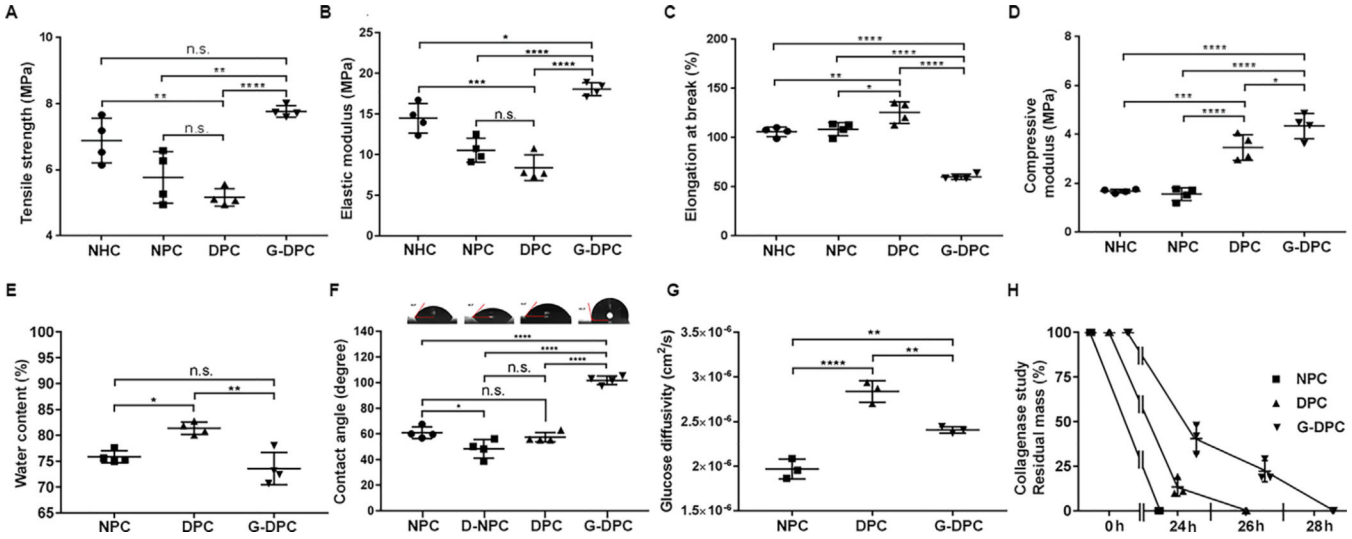

Fig. 4.

Mechanical and functional assessment of decellularized and sterilized porcine corneas. (A–D) Mechanical properties comparison among native human cornea (NHC), native porcine cornea (NPC), decellularized porcine cornea (DPC) and gamma irradiated decellularized porcine cornea (G-DPC). (E–H) Functional characteristic comparison among different cornea samples. (F) Micrographs of water contact angle of different corneas placed on the top of their respective group's contact angle measurement graph; D-NPC: deepithelialized NPC. (H) For the collagenase study, residual masses are presented against time in hours (h). For all panels, quantitative results were reported as the mean ± S.D. from four independent corneas and results were compared between groups.

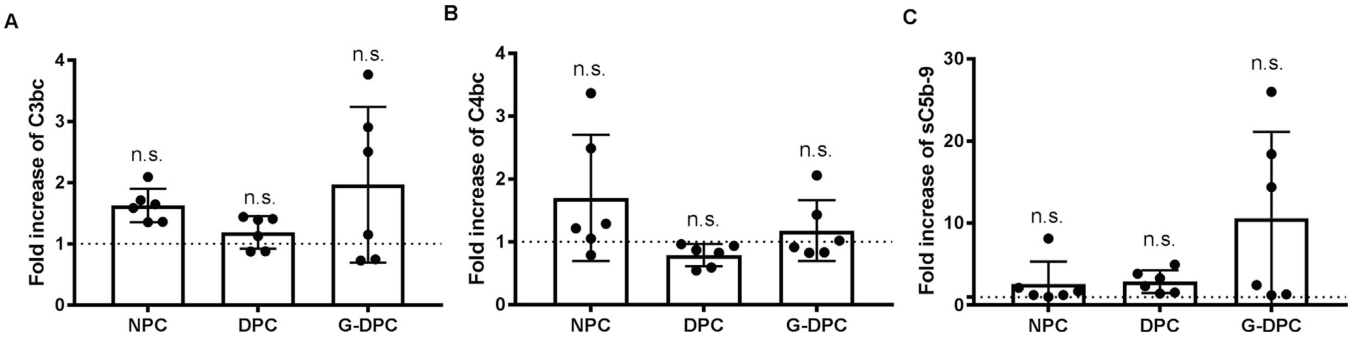

Fig. 5.

Complement activation induced by native porcine cornea (NPC), decellularized porcine cornea (DPC) and gamma irradiated decellularized porcine cornea (G-DPC) after incubation in normal human plasma for 30 min at 37 °C. (A) C3-activation (C3bc), (B) C4-activation (C4bc) and (C) terminal pathway activation (sC5b-9) are reported as fold increase relative to the background activation in plasma without a cornea (indicated with a dotted line). The bars show mean fold increase ± S.D. of six independent corneas. n.s.: non-significant.

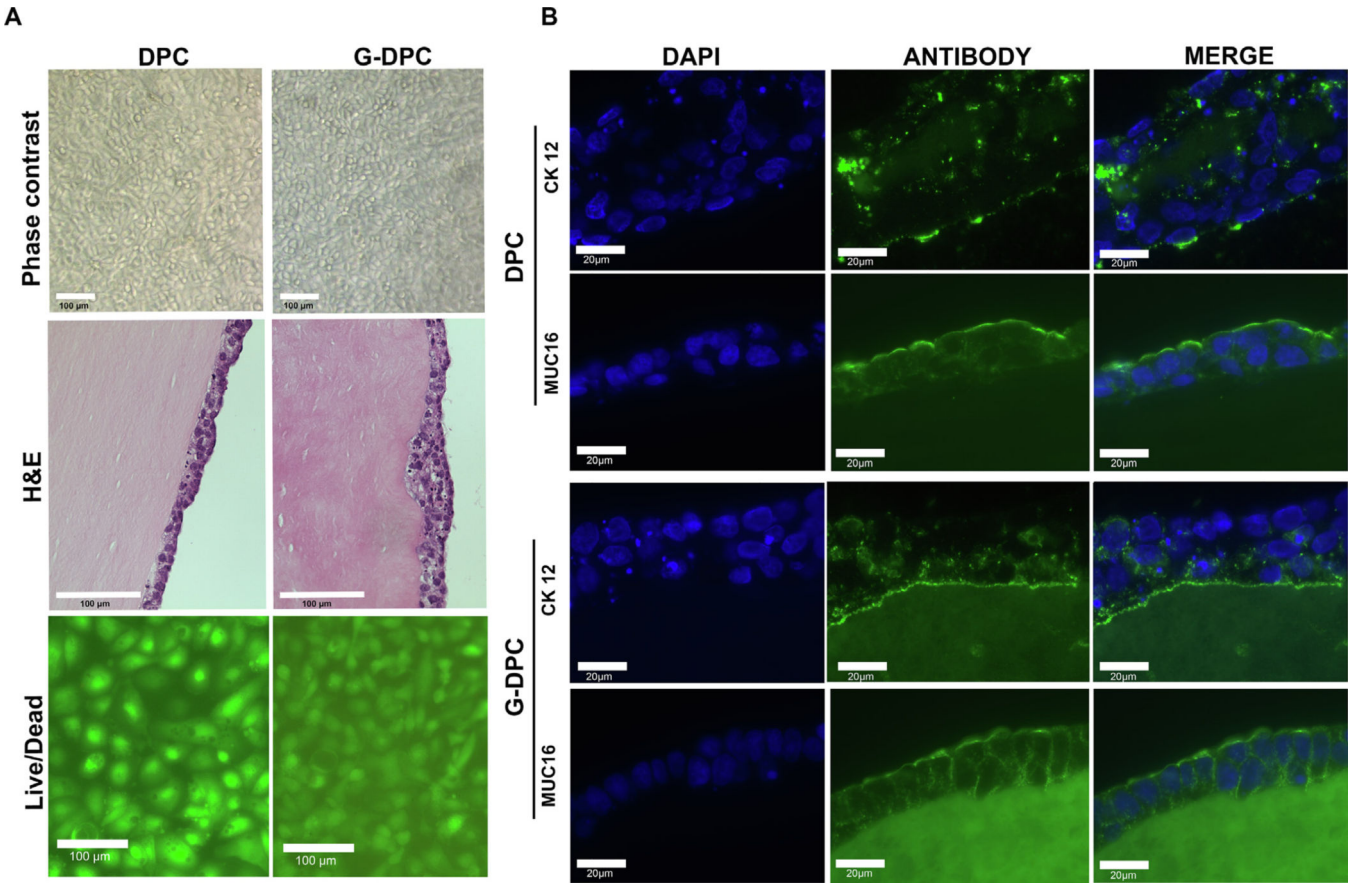

Fig. 6.

Evaluation of the recellularization process. (A) Corneal epithelial recellularization on decellularized porcine cornea (DPC) and gamma irradiated decellularized porcine cornea (G-DPC), showing cell monolayers by phase contrast microscopy and stratified epithelia by Hematoxylin and Eosin (H&E) staining on the anterior surface of DPC and G-DPC. Live/dead staining for cytotoxicity: green cells are live and red cells are dead. Scale bars: 100 µm. (B) Representative fluorescence microscopy images for the expression of cytokeratin 12 (CK12) (green) and mucin (MUC16) (green) by human corneal epithelial cells on DPC and G-DPC. Nuclei were stained with DAPI (blue). Scale bars: 20 µm.

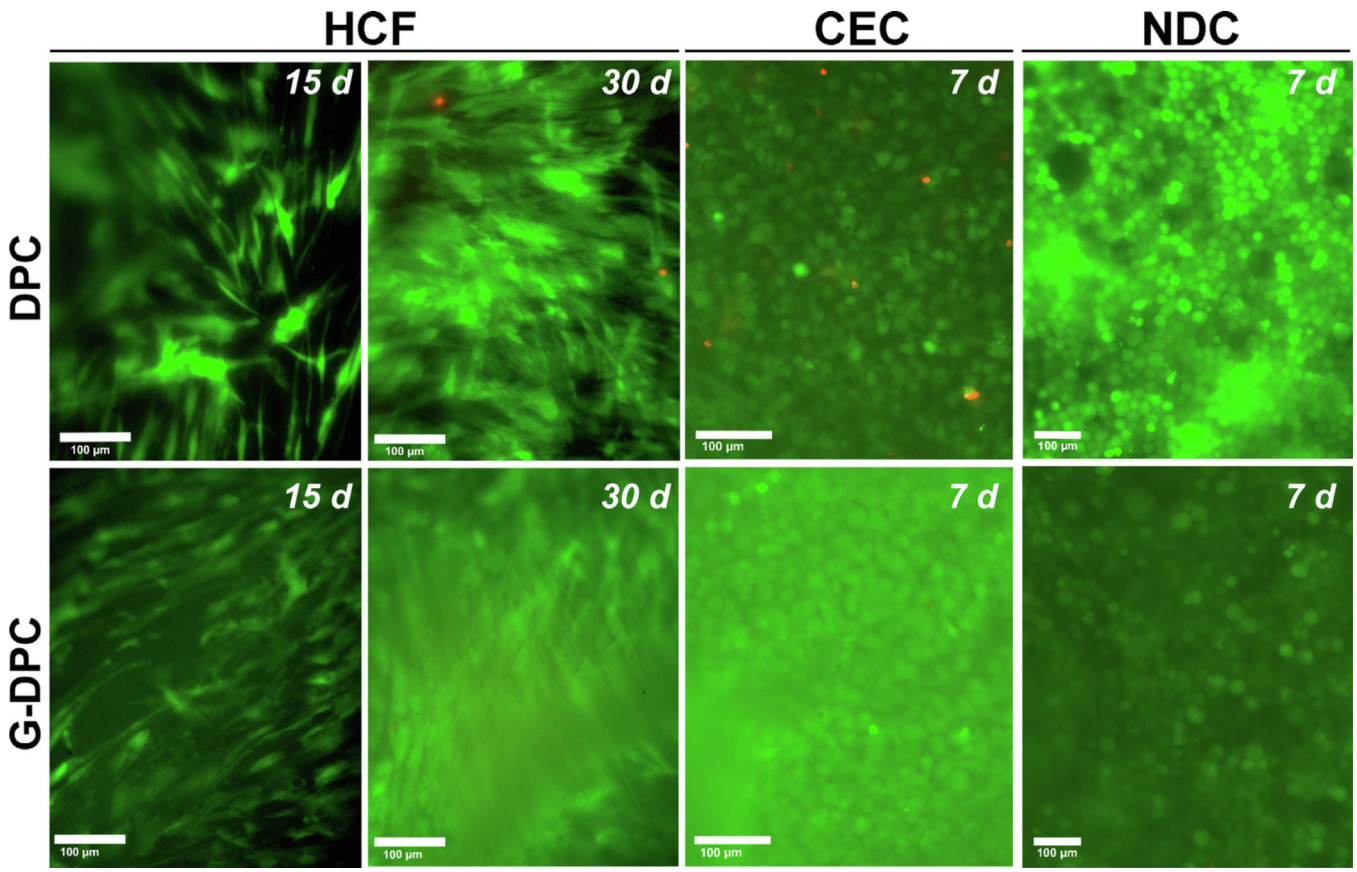

Fig. 7.

Live/dead staining of human corneal fibroblasts (HCF), human corneal endothelial cells (CEC) and neural progenitor cells (NDC) on decellularized porcine cornea (DPC) and gamma irradiated decellularized porcine cornea (G-DPC). Numbers inside the panels indicate the culturing time in days. Scale bars: 100 µm.

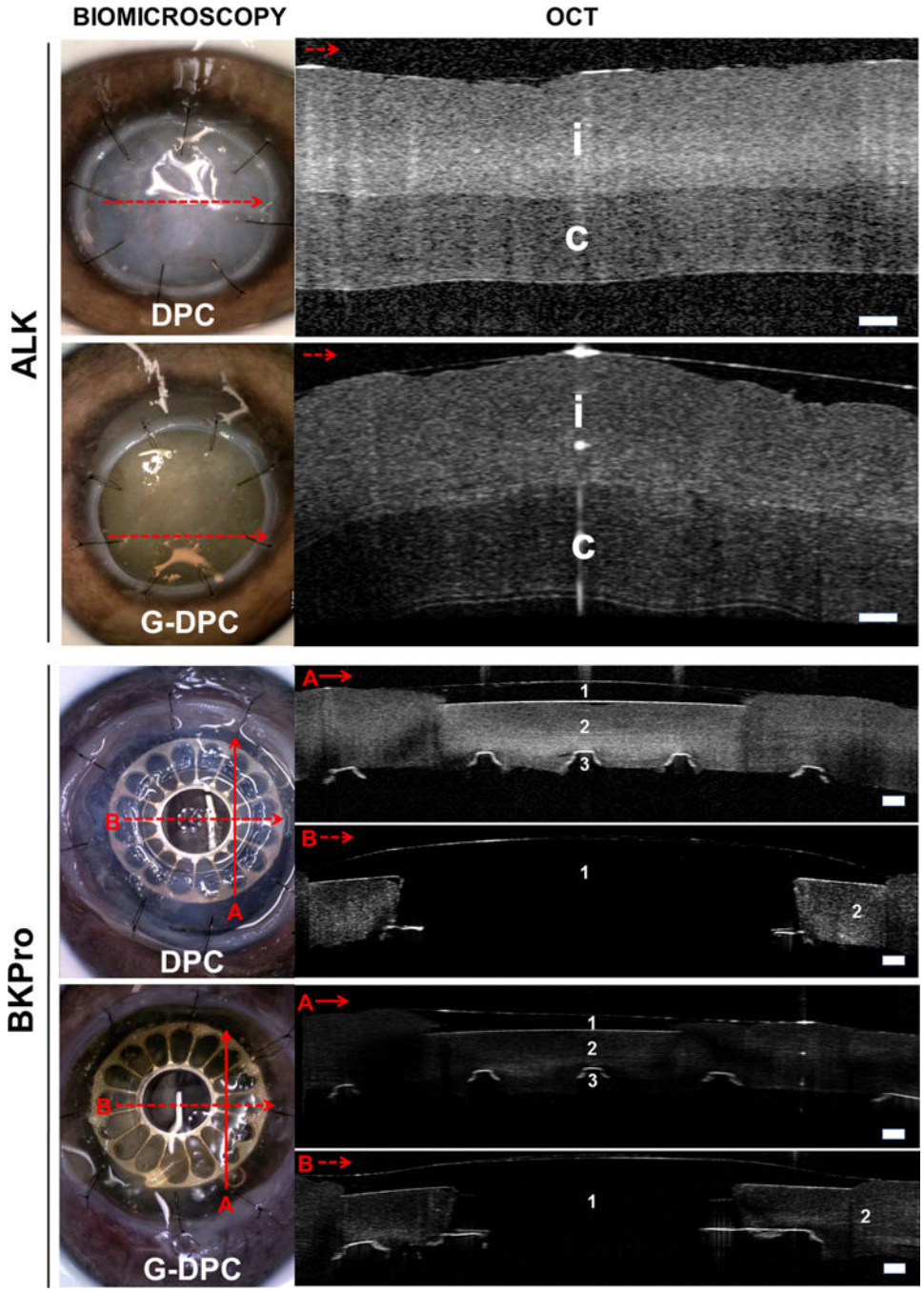

Fig. 8.

Biomicroscopy and OCT images of non-gamma (DPC) and gamma irradiated (G-DPC) decellularized porcine corneas transplanted ex vivo in pig eye as anterior lamellar grafts and as a carrier for BKPro. Red arrows on the slit lamp images represent the section and direction of the OCT. No gaps within implanted donor cornea (i) or host corneas (c) were observed in either model. 1, 2 and 3 represent BKPro front plate (made of PMMA), donor cornea and BKPro black plate (made of titanium), respectively. Scale bars: 200 μm.